NASA TECHNICAL MEMORANDUM

NASA TM X-2221

NASA TM X-2221

FLIGHT TESTS OF CROSS, MODIFIED RINGSAIL, AND DISK-GAP-BAND PARACHUTES FROM A DEPLOYMENT ALTITUDE OF 3.05 km (10 000 ft)

by Clinton V. Eckstrom and Harold N. Murrow

Langley Research Center
Hampton, Va. 23365

NATIONAL AERONAUTICS AND SPACE ADMINISTRATION • WASHINGTON, D. C. • JUNE 1971

1. Report No.	2. Government Accession No.	3. Recipient's Catalog No.
NASA TM X-2221		

4. Title and Subtitle	5. Report Date
FLIGHT TESTS OF CROSS, MODIFIED RINGSAIL, AND DISK-GAP-BAND PARACHUTES FROM A DEPLOYMENT ALTITUDE OF 3.05 km (10 000 ft)	June 1971
	6. Performing Organization Code

7. Author(s)	8. Performing Organization Report No.
Clinton V. Eckstrom and Harold N. Murrow	L-7389
	10. Work Unit No.
	709-12-00-01

9. Performing Organization Name and Address	11. Contract or Grant No.
NASA Langley Research Center Hampton, Va. 23365	
	13. Type of Report and Period Covered
	Technical Memorandum

12. Sponsoring Agency Name and Address	14. Sponsoring Agency Code
National Aeronautics and Space Administration Washington, D.C. 20546	

15. Supplementary Notes

16. Abstract

Eleven parachute flight tests were conducted at the Department of Defense Joint Parachute Test Facility, El Centro, California. These tests were made to obtain low-altitude deployment and performance data on cross, modified ringsail, and disk-gap-band (DGB) parachutes that had previously been flight tested at earth altitudes above 30.5 km (100 000 ft). Parachute details, flight test conditions, opening loads, and performance data are presented for each of the flight tests. For seven of the flight tests, structural load data are presented as obtained from miniature load cells installed at various points in the suspension lines and canopy of each of the three parachute configurations.

17. Key Words (Suggested by Author(s))	18. Distribution Statement
Parachute loads Parachute performance Decelerators	Unclassified – Unlimited

19. Security Classif. (of this report)	20. Security Classif. (of this page)	21. No. of Pages	22. Price*
Unclassified	Unclassified	57	$3.00

*For sale by the National Technical Information Service, Springfield, Virginia 22151

FLIGHT TESTS OF CROSS, MODIFIED RINGSAIL, AND DISK-GAP-BAND PARACHUTES FROM A DEPLOYMENT ALTITUDE OF 3.05 km (10 000 ft)

By Clinton V. Eckstrom and Harold N. Murrow
Langley Research Center

SUMMARY

Eleven parachute flight tests were conducted at the Department of Defense Joint Parachute Test Facility, El Centro, California. These tests were made to obtain low-altitude deployment and performance data on cross, modified ringsail, and disk-gap-band (DGB) parachutes that had previously been flight tested at earth altitudes above 30.5 km (100 000 ft). Parachute details, flight test conditions, opening loads, and performance data are presented for each of the flight tests. For seven of the flight tests, structural load data are presented as obtained from miniature load cells installed at various points in the suspension lines and canopy of each of the three parachute configurations.

INTRODUCTION

The National Aeronautics and Space Administration has recently completed an experimental flight test program (ref. 1) which provided performance data for several parachute configurations that might be utilized for applications in low-density atmospheres. The flight tests were conducted in the earth's atmosphere at deployment altitudes ranging from 37.3 to 48.3 km (122 500 to 158 500 ft). The parachute designs tested were the disk-gap-band (DGB), modified ringsail, and cross parachutes.

A series of low-altitude tests at the Department of Defense Joint Parachute Test Facility, El Centro, California, was initiated to obtain deployment and performance data on the same parachute designs that had previously been flight tested at the higher earth altitudes. The primary objective of these 11 flight tests was to obtain low-altitude data on parachute deployment dynamics and steady-state drag and stability. For the first two flight tests, a secondary objective was to evaluate the capability of the parachutes to operate in the low-altitude test environment selected. For the next seven flight tests, the secondary objective was to demonstrate the flightworthiness of small load cells installed in the parachute canopies and suspension members (ref. 2). The secondary objective of the last two flight tests was to evaluate an energy absorber system located in the parachute

suspension system and determine its applicability for future high-altitude parachute deployment tests. The energy absorber would be utilized to reduce the magnitude of the opening shock load transmitted to the payload.

Additional objectives of these tests include (1) determination of a method to retain the parachute deployment bag and mortar lid with the parachute to prevent it from becoming a flying object which could damage the parachute canopy, (2) evaluation of modifications to the deployment mortar system, and (3) documentation of the parachute "settling" motion after ground impact of the payload to evaluate (for future applications) the possibility of interference of an attached parachute with the operation of a scientific payload.

SYMBOLS

Values are given in both SI and U.S. Customary Units. The measurements and calculations were made in U.S. Customary Units.

a_t total acceleration, dV_t/dt, m/sec^2 (ft/sec^2)

$C_{D,o}$ drag coefficient based on nominal canopy surface area S_o and total velocity V_t

$(C_{D,o})_{eff}$ effective drag coefficient (based on vertical descent velocity $\dot{z}$)

D_o nominal diameter, $\left(\frac{4S_o}{\pi}\right)^{1/2}$, m (ft)

g acceleration due to gravity, 9.81 m/sec^2 (32.2 ft/sec^2)

L/D lift-drag ratio

q_∞ free-stream dynamic pressure, N/m^2 (lbf/ft^2)

S_o nominal surface area of parachute canopy including geometric open areas within borders of cloth material (cross parachute has no geometric open areas by this definition), m^2 (ft^2)

S_p projected canopy area, m^2 (ft^2)

$S_{p,final}$ projected canopy area during steady-state descent, m^2 (ft^2)

t	time, sec
t'	time from mortar firing, sec
V_t	total velocity (measured velocity corrected for horizontal winds), m/sec (ft/sec)
W	total system weight, kg (lbm)
$\dot{x}$	velocity component along X-axis (positive north) of range coordinate system, m/sec (ft/sec)
$\dot{y}$	velocity component along Y-axis (positive east) of range coordinate system, m/sec (ft/sec)
$\dot{z}$	velocity component along Z-axis (positive up) of range coordinate system, m/sec (ft/sec)
ρ	atmospheric air density, kg/m^3 ($slugs/ft^3$)

Subscripts:

ad	adjusted
adv	adjusted average
meas	measured
std.sl	standard sea level

TEST FACILITY AND SUPPORTING EQUIPMENT

The tests were conducted with the assistance of the U.S. Air Force 6511th Test Group (Parachute) and the Naval Aerospace Recovery Facility personnel at the Department of Defense Joint Parachute Test Facility at the Naval Air Facility, El Centro, California, where an instrumented test range and other required support personnel and equipment were available. All the drop tests were initiated at an altitude near 3.05 km (10 000 ft). These tests were conducted over the Foothill Drop Zone with a network of theodolite camera stations (fig. 1) for obtaining trajectory data. Photographic coverage included a 16-mm camera on the instrumented payload, a 16-mm camera in a chase airplane, and

four 16-mm cameras at the Master Control Center at the Foothill Drop Zone with focal lengths varying from 2.54 cm (1 in.) to 152.4 cm (60 in.). Some 70-mm sequence stills were obtained from a ground station, and for some flight tests 16-mm camera coverage was obtained of the parachute collapse sequence at the impact area. Surface meteorological conditions were monitored at the Master Control Center and atmospheric data to 3.05 km (10 000 ft) were obtained from a Rawin sounding made near the time and location of each drop test. The first two flight tests were initiated from a C-130 airplane with an inert payload configuration. The remaining flight tests were made from a T-33 airplane with the instrumented payload mounted as a store beneath the wing prior to release, as shown in figure 2.

TEST ITEMS

Parachutes

The 9.1- to 12.2-m-nominal-diameter (30 to 40 ft) parachutes flight tested in this program had either been flight tested previously on the rocket launch portion of the high-altitude test program summarized in reference 1 or were spare parachutes which were identical to those which were actually flight tested. Therefore, considerable details of the construction and configuration of these parachutes is available in references 3 to 8, as well as high-altitude flight performance data. Photographs of the three types of test parachutes are presented in figures 3(a) to 3(c), and dimension and construction details are presented in table I. (There were five variations of size and type of parachutes with a total of six parachutes being used.) A cross parachute, a disk-gap-band (DGB) parachute, and a modified ringsail parachute were equipped with seven miniature load cells. (See figs. 4, 5, and 6.)

Details of the load cells and an evaluation of their use are presented in reference 2. Although these instruments were included in the flight tests primarily to evaluate their performance for possible use on future high-altitude flight tests, the loads measured are presented so that this limited amount of data will be available to potential users.

Payload

The test payloads for flight tests 1 and 2 were each inert weights of 272 kg (600 lbm). A photograph from flight test 1 (fig. 3(b)) shows the payload-parachute descent configuration. The test payload for flight tests 3 to 11 was a cylindrical vehicle with a conical nose and fins (fig. 7). The payload was equipped with two ballast chambers so that the total system weight could easily be varied from 181 kg (400 lbm) for flight tests 3 to 7 to 272 kg (600 lbm) for flight tests 8 to 11. The payload was also provided with an eight channel telemetry system for transmission of data. There were seven channels for data from the

miniature load cells in the parachute and one channel for data from the main tensiometer used to measure total loads in the attachment riser system. For the last two flight tests only the main tensiometer was used. For each test the packed parachute was located in the deployment mortar at the aft end of the payload. Prior to deployment, the parachute riser and bridle lines and the main tensiometer were located in storage areas on the outside surface of the mortar tube but inside the payload shell. For the last two flight tests, the energy absorber system was also similarly located outside the mortar tube. The deployment system was essentially the same as that used on the rocket-launched payloads (ref. 7) with the exception of the mortar sabot which was changed from a dish type to a cup type (fig. 8). An additional change which occurred during the tests was the shortening of the mortar tube by 7.6 cm (3 in.). This change was to eliminate the necessity of placing a balsa spacer block in the interior of the parachute deployment bag to maintain a parachute packing density of approximately 640 kg/m^3 (40 lbm/ft^3) for the smaller and/or lighter weight parachutes. The deployment bag was firmly attached to the apex of the test parachute and the mortar system lid was attached to the closed end of the deployment bag. For the last two flight tests the mortar lid was "skeletonized" to reduce its weight. Figure 9 shows the original lid design with two examples of skeletonized lids used for subsequent high-altitude tests.

TESTING TECHNIQUE

The first two flight tests used an inert payload which was released from the open tail gate of a C-130 airplane with deployment of the parachute initiated by a 9.1-m (30 ft) lanyard as depicted by the sketch in figure 10. For the remaining nine flight tests, the instrumented payload was dropped from a T-33 airplane by the wing-mounted store-release system. Two short lanyards attached to the airplane pulled two pins as the payload dropped away. One pin armed the payload mortar system and the other activated the payload timer system. The payload timer started the payload camera immediately and was set to fire the parachute deployment mortar 3 sec after the payload was released from the airplane. This time allowed sufficient separation of the payload from the airplane to avoid any possible damage to the airplane. A schematic of this deployment sequence is shown in figure 11.

After the deployment mortar fired, the parachute riser, tensiometer, and bridle in that sequence were deployed from the storage areas outside the mortar tube. As the riser-bridle system was elongated to full length, a circular knife (on the riser) cut the cord holding the deployment bag closed and allowed the parachute suspension lines to deploy full length and then the canopy. On the previous high-altitude flight tests, the bag and lid combination was allowed to separate from the main canopy after deployment was completed. However, in some instances (ref. 3) the trajectory of the free-flying bag and

lid combination intersected with that of the more rapidly decelerating main parachute; this resulted in a collision and significant damage to the main parachute canopy. Therefore, for these flight tests the bag and lid combination was designed to remain attached to the parachute canopy apex after deployment was completed. Various attachment methods were investigated.

FLIGHT TESTS

As mentioned previously, 11 flight tests were conducted with cross, modified ringsail, and disk-gap-band parachutes ranging in nominal diameter from 9.1 to 12.2 m (30 to 40 ft). For all the flight tests, the primary purpose was to observe deployment dynamics and steady-state stability and drag performance. Test conditions are presented in table II, and performance data are presented in table III.

Accuracy of Data

The system weights presented in table II are considered accurate to within ±1 percent. The release velocities listed in table II are those requested for the flight tests. The actual total velocities, the release altitudes, and the dynamic pressures at the time of payload release, along with the mortar delay times and the dynamic pressures at the time of mortar firing, are also presented in table II. These data were derived from theodolite space position data and from meteorological conditions determined by the Rawin sounding made at or near the time of the flight test. The surface meteorological conditions listed were those recorded at the Master Control Center at the drop zone at the start of each flight test. The test times listed are the times of release of the payload from the airplane. As shown in table II, the rawinsonde release time was near the payload release time for most of the flight tests. An exception is flight test 5 where meteorological data were not obtained from the scheduled rawinsonde release at 8:45 a.m. PDT (27 min after payload release). Because the expected rawinsonde data were not available, data were used from the next Rawin sounding made at 10:05 a.m. PDT or 1 hr and 47 min after the flight test.

In table III, the time intervals from mortar firing to line stretch and to maximum load were determined from the telemetered tensiometer data and are believed to be accurate to within ±0.02 sec. The time intervals listed in table III for the first canopy opening and the stable canopy opening were determined from either the payload, chase airplane, or ground-based camera films and are accurate to about ±0.2 sec. The opening distances (ref. 9) listed in table III were determined from the velocity histories during the opening time intervals and are accurate to about ±5 percent. The ground impact times were determined from the theodolite film data and are accurate to within ±1 sec.

The deployment load data presented in table III were obtained from mechanical tensiometers for the first two inert payload drop tests and from the telemetered tensiometer data for the remaining flights. For flight test 9, the telemeter channel for the main tensiometer was not operative and, therefore, the total load was estimated on the basis of load values measured in three of the 36 suspension lines. The data from the mechanical tensiometers are considered accurate to within ±10 percent, whereas those from the telemetered tensiometers are considered accurate to within ±3 percent. The estimated total load for flight test 9 is believed to be accurate to within ±20 percent.

Analysis Methods

In table III, the average values of the rate of descent adjusted to standard sea-level density condition are based on descent rate reduced from theodolite data and Rawin sounding measurements of atmospheric density as follows:

$$(\dot{z})_{ad} = \left(\frac{\rho_{meas}}{\rho_{std.sl}}\right)^{1/2} \dot{z}_{meas}$$

The average values of effective drag coefficient $(C_{D,o})_{eff}$ presented in table III are determined from the average rate of descent adjusted to standard sea-level density condition as follows:

$$(C_{D,o})_{eff} = \frac{2W}{S_o(\rho_{std.sl})(\dot{z}_{adv})^2}$$

The average value of $C_{D,o}$ presented in table III was determined by the following equation:

$$C_{D,o} = \frac{W}{S_o \frac{1}{2}\rho V_t^2}\left(\frac{a_t}{g} + \frac{\dot{z}}{V_t}\right)$$

For the drop tests conducted, the wind drift often caused the horizontal velocity of the test item to be equal to or greater than the vertical velocity during steady-state descent. Therefore, the correction for horizontal winds is important since relatively small errors in wind correction could result in large uncertainties in the $C_{D,o}$ data. The lift-drag ratio L/D was obtained from the following equation:

$$\frac{L}{D} = \frac{\left(\dot{x}^2 + \dot{y}^2\right)^{1/2}}{\dot{z}}$$

where the horizontal velocity components have been corrected for wind by subtracting out the wind velocity.

The average value of the parachute angle off vertical was determined directly from theodolite data.

The dynamic-pressure histories presented in the data figures for the 3-sec period immediately after mortar firing are values calculated by using velocity data obtained by differentiation of smoothed positional data from the theodolite recordings. The actual system velocity was changing rapidly during this period and therefore large errors were introduced into the calculated values of velocity because of the smoothing process used. The dynamic-pressure values shown are accurate only to within ±15 percent during the period of large change but are accurate to about ±4 percent at the beginning and end of this period.

RESULTS AND DISCUSSION

Preliminary Drop Tests

Prior to use of the instrumented payload, two drop tests were performed with an inert payload to qualify the previously used parachute systems for the low-altitude environment selected for these tests. A 9.1-m-nominal-diameter (30 ft) DGB parachute similar to that described in reference 4 was used in the first preliminary drop test (flight test 1). For the deployment sequence, depicted in figure 10, the parachute opened quickly and withstood the maximum opening load of 26 910 N (6050 lbf) with no damage. During descent, the parachute average adjusted rate of descent was 12.3 m/sec (40.3 ft/sec) for an average $(C_{D,o})_{eff}$ of 0.48. The average angle off vertical as determined from film data was 12.7°. An average $C_{D,o}$ of 0.46 and an average L/D of 0.14 were determined from this preliminary test. Because this first test parachute withstood the opening loads encountered without damage, the tests proceeded as planned.

The second preliminary drop test with an inert payload (flight test 2) used a 12.2-m-nominal-diameter (40 ft) modified ringsail parachute. This particular parachute was fabricated of cloth having much greater than normal air permeability as shown in table I. This parachute had failed to inflate in a previous high-altitude, high-velocity rocket-launched test (ref. 5). It was determined after the high-altitude test that the most probable cause of the original failure to inflate was that the total porosity (geometric porosity and cloth permeability) was greater than allowable for the crown area of the canopy. However, the payload had been spinning at deployment on the high-altitude flight test; this resulted in twisting of the suspension lines which may have contributed to the opening difficulties. Therefore, it was desirable to test this parachute again at a lower deployment velocity and with a nonspinning payload. This modified ringsail parachute with its inert payload was also deployed from the C-130 airplane as depicted in figure 10. For this flight test, the deployment sequence was normal through line stretch and bag strip but

again the canopy only partially inflated even without the influence of twisted suspension lines. Thus, the failure of this modified ringsail parachute to inflate was definitely attributed to excessive total porosity in the crown area of the canopy. No further flight tests were planned with this parachute.

Instrumented Parachute Tests

Flight tests 3 to 9 were made with the instrumented payload and with a 9.1-m-nominal-diameter (30 ft) cross parachute, a 12.2-m-nominal-diameter (40 ft) disk-gap-band parachute, and a 9.5-m-nominal-diameter (31.2 ft) modified ringsail parachute each of which was instrumented with seven miniature load cells as shown in figures 4, 5, and 6, respectively. The miniature load cells, which were monitored on a continuous basis, measured the load distribution on each of the three parachutes during the deployment and inflation process. The tests were made to evaluate the instrumentation (ref. 2) as well as to collect usable design data.

Cross parachute.- Three drop tests (flight tests 3, 7, and 9) were performed with the 9.1-m-nominal-diameter (30 ft) cross parachute with load cells on the canopy tapes and in the suspension lines (fig. 4). Note that there are five load cells on the continuous load path formed by suspension line 5, canopy tape 5 which becomes canopy tape 23 as it crosses the midpoint of the canopy, and suspension line 23.

For flight test 3 where the system weight was 177 kg (390 lbm) the cross parachute deployed and opened properly as shown in payload camera photographs (fig. 12). The parachute projected-area ratio, the dynamic pressure, and the total force encountered during the first 3 sec of the deployment and inflation process are shown in figure 13, and the recordings from the load cells on the canopy tape and in the suspension lines are presented in figure 14. A record was not received from the load cell on canopy tape 23; also, the load cell on canopy tape 28 experienced torsional overload during the data period. The remaining four load cells on the continuous load path formed from lines and tapes 5 and 23 registered maximum loads ranging from 530 N (119 lbf) to 765 N (172 lbf). There was a maximum load of 380 N (85 lbf) recorded at the bottom of line 1, which goes to the outside edge of a panel arm, and a maximum load of 625 N (140 lbf) recorded at the bottom of line 5, which goes to the center line of the same panel arm. Unpublished data from previous wind-tunnel tests also indicated that the load along the outer edges of a panel arm was less than that in the center of the panel arm. The individual maximum recorded suspension line and canopy tape loads varied from 85 percent to 172 percent of the average calculated load per line based on the maximum total load of 16 015 N (3600 lbf) and a total of 36 suspension lines and canopy tapes.

For flight test 7, the second for the instrumented cross parachute, the total system weight was 179 kg (394 lbm). The cross parachute again deployed and opened properly

as shown by photographs from ground-based cameras (fig. 15). Figure 16 presents time histories of the parachute projected-area ratio, the dynamic pressure, and the total force for flight test 7. The recordings from the canopy tape and suspension line load cells are shown in figure 17. Valid data were received from three load cells. The maximum loads recorded ranged from 465 N (104 lbf) on canopy tape 28 along the edge of a panel arm to 800 N (180 lbf) on canopy tape 5 at the center line of the panel arm. This range gives a load variation from 74 to 127 percent of the average calculated load per line based on the maximum total load of 22 685 N (5100 lbf) and a total of 36 suspension lines and canopy tapes.

For flight test 9, the third flight test of the instrumented cross parachute, the total system weight was increased to 272 kg (600 lbm). Again the cross parachute deployed and opened properly as shown in payload camera photographs (fig. 18). Figure 19 presents time histories of the parachute projected-area ratio and the dynamic pressure for flight test 9. Figure 20 presents the recordings from the seven canopy tape and suspension line load cells for the first 3 sec after mortar firing. Unfortunately, the telemetry channel for the total load became inoperative at mortar firing for this flight test. The five load cells on the continuous load path along the center line of a panel formed from lines and tapes 5 and 23 registered maximum loads varying from 780 N (175 lbf) on canopy tape 23 to 1045 N (235 lbf) at the bottom of suspension line 5. Again, the loads at the outer edges of the panels, as exemplified by the load on suspension line 1 of 710 N (160 lbf) and on canopy tape 28 of 690 N (155 lbf) were less than loads along the panel center line. However, suspension lines 1 and 5 became entangled during the deployment process and remained entangled during the data period shown in figure 20; this entanglement may have influenced the loads measured in these two lines. As seen in figure 20, the loads registered at all load cells were significant for a fairly long time period, $t' = 0.8$ to 1.4 sec. The maximum total opening load was estimated to be approximately 31 140 N (7000 lbf) based on the average of loads measured in three individual suspension lines.

For the three drop tests of the instrumented cross parachute, the average drag coefficient ranged from 0.58 for flight test 7 to 0.74 for flight test 9. (See table III.) The average effective drag coefficient was slightly higher and varied from 0.70 for flight test 3 to 0.76 for flight test 9. The lift-drag-ratio range was from 0.14 for flight test 9 to 0.39 for flight test 7. The average angle off vertical ranged from 1.8° for flight test 9 to 4.4° for flight test 7. As mentioned previously, the values of $(C_{D,o})_{eff}$ and average angle off vertical are obtained from direct measurements, whereas the values of $C_{D,o}$ and L/D are measurements corrected for winds determined from a Rawin sounding made near the time of the drop test. The wind-corrected data for flight tests 3 and 9 agree with results from the previous high-altitude flight test (ref. 6); whereas, the data for flight test 7 indicate a lower $C_{D,o}$ and a higher L/D than expected.

Modified ringsail parachute.- Two drop tests (flight tests 4 and 6) were performed with the 9.5-m-nominal-diameter (31.2 ft) modified ringsail parachute with load cells on the canopy and in the suspension lines (fig. 6). During flight test 4, the modified ringsail parachute deployed and opened properly as shown by photographs from ground-based cameras (fig. 21). During the opening process, the canopy encountered a maximum opening load of 24 910 N (5600 lbf) with only minor canopy damage and one broken suspension line. As can be seen from table I, the maximum design or "safe opening" load for this parachute was only 18 325 N (4120 lbf). Figure 22 presents time histories of parachute projected-area ratio, dynamic pressure, and total force.

For this flight test, the canopy overinflation process (or the shape distortion due to wake effects of the rapidly decelerating system) began immediately after the time of maximum opening load and before the canopy was fully inflated the first time (fig. 22). Figure 23 presents the recordings from load cells installed on the canopy and in the suspension lines. Suspension lines 11 and 23 recorded maximum loads of 1025 and 815 N (230 and 183 lbf), respectively. The average load per line based on the maximum opening load was 1035 N (233 lbf). On the instrumented panels in the canopy, all load cells apparently functioned properly; however, only the load cell at the upper edge of sail 5 recorded any significant load (580 N (130 lbf) maximum load). The electrical cable to the load cell on the upper edge of sail 6 was on the suspension line that broke (line 22); this resulted in loss of data from that instrument.

For the second drop test of this parachute (flight test 6), the payload release velocity was reduced from 150 to 120 knots indicated airspeed to reduce the parachute opening load. Although the parachute deployed and opened as shown in figure 24 (photographs from the payload camera), the opening load was only slightly reduced (22 240 N (5000 lbf)) and 15 of the 24 suspension lines failed. Also, extensive damage occurred to several canopy sail panels as shown in figure 25. This canopy damage occurred after the suspension lines failed but was evident during the latter portion of the canopy collapse sequence. Figure 26 presents time histories of the parachute projected-area ratio, dynamic pressure, and total force for flight test 6. Figure 27 presents the recordings from the canopy and suspension line load cells. The maximum loads recorded at the top and bottom of suspension line 23 at the time of line failure were 1240 and 1225 N (279 and 275 lbf) and the load histories are nearly identical. The average load per line for this flight based on the maximum opening load was 925 N (208 lbf). The maximum load on suspension line 23 was substantially greater than the calculated average and was also greater than that recorded on flight test 4 where very little parachute damage was noted. Suspension line 23 was the middle line of the 15 suspension lines that broke and suspension line 11, which recorded a maximum load of 910 N (205 lbf) was the middle line of the nine lines which remained intact. The top edge of sail 5 recorded a maximum load of 140 N (32 lbf). Records were not obtained from the top edges of sails 7 and 9 because of telemetry

malfunction and from sail 10 because that load cell had been removed and relocated at the upper end of suspension line 23.

Performance data (table III) from the first drop test (flight test 4) of the modified ringsail parachute indicate an average $C_{D,o}$ of 0.55. The average $(C_{D,o})_{eff}$ based on vertical descent velocity was 0.63, which was somewhat higher than that obtained in an earlier high-altitude flight test (ref. 7). The average L/D was 0.36 and the average angle off vertical was 6.8°. Again, it is to be noted that the values of $(C_{D,o})_{eff}$ and the angle off vertical are obtained from direct measurements, whereas the values of $C_{D,o}$ and L/D are measurements corrected for winds determined from a Rawin sounding made near the time of the drop test.

Disk-gap-band parachute.- Two drop tests (flight tests 5 and 8) were performed with the 12.2-m-nominal-diameter (40 ft) DGB parachute with load cells on the canopy tapes and in the suspension lines (fig. 5). During flight test 5, the DGB parachute deployed and opened properly as shown in figure 28. Time histories of the parachute projected-area ratio, dynamic pressure, and total force are presented in figure 29. Recordings from the canopy tape and suspension line load cells are presented in figure 30. The maximum opening load encountered was 19 570 N (4400 lbf) for an average load per line of 615 N (138 lbf). The maximum load recorded in suspension line 32 was 310 N (70 lbf) and on the opposite side of the canopy in radial tape 16 the maximum recorded load was 780 N (175 lbf). No significant loads were measured at the top and bottom edges of the band and this would be expected since that part of the canopy had not inflated during the time period that maximum loads were encountered.

This parachute was used again in flight test 8. Photographs showing the parachute deployment, initial opening, and subsequent canopy line failure are presented as figure 31. For this flight test, the payload timer apparently had been improperly cycled during the checkout prior to the test; this resulted in a time delay of 14.24 sec between release from the airplane and mortar firing rather than the nominal 3 sec planned. The excess free fall time allowed the payload to accelerate due to gravity so that the dynamic pressure increased from an expected value of 3590 N/m^2 (75 lbf/ft^2) to a maximum value of 8830 N/m^2 (184.4 lbf/ft^2) as shown in table II. The maximum opening load recorded prior to canopy failure was 28 025 N (6300 lbf) as noted in table III and figure 32. This load gives an average load per line of 875 N (197 lbf). Force records were obtained from the two load cells in suspension lines 16 and 32, with maximum loads being 1595 N (359 lbf) in line 32 and 1045 N (235 lbf) in line 16. (See fig. 33.) The canopy failure mode was from a rip that started in gore 11 near the apex of the canopy and traveled down to the skirt, across 12 suspension lines (lines 11 through 1 and line 32), and up gore 31 to the apex again. This rip caused an entire section (12 gores of 32) of the canopy to trail behind the parachute in addition to causing the complete collapse of the remainder of the canopy.

Performance data (table III) from the first drop test (flight test 5) of the 12.2-m (40 ft) DGB parachute indicated an average $C_{D,o}$ of 0.37. The average $(C_{D,o})_{eff}$ based on vertical descent velocity was 0.55. The average L/D was 0.57 and the average angle off vertical was 6.8°. The values shown for $(C_{D,o})_{eff}$ and the angle off vertical compare well with previous flight-test data as reported in reference 8. However, the average $C_{D,o}$ and the average L/D which are corrected for measured winds appear to be significantly different from the values expected on the basis of previous experience. A check of the wind conditions used to make corrections to the flight data revealed that the wind data were not obtained from the rawinsonde released near the time of the drop test and that wind data were used from the next available sounding which was 1 hr and 47 min after the drop test. Because the wind data used in the parachute performance data corrections were not obtained within a close time interval, the $C_{D,o}$ and L/D data shown in table III for flight test 5 are considered to be of questionable value.

Energy-Absorber Tests

The last two drop tests (flight tests 10 and 11) with a 9.1-m-nominal-diameter (30 ft) cross parachute were for the purpose of evaluating an energy absorbing system being developed for use in a rocket-launched flight test. Details of the energy absorber are presented in reference 10 and results of the rocket-launched flight test are reported in reference 11.

Photographs from a ground-based camera showing the deployment and opening of the cross parachute on flight test 10 are presented as figure 34. Time histories of the parachute projected-area ratio, dynamic pressure, and total force are given in figure 35. Photographs from the payload camera showing the deployment and opening sequence during flight test 11 are presented as figure 36. The energy-absorber material can also be seen in figure 36. Time histories of the parachute projected-area ratio, dynamic pressure, and total force are given in figure 37. During the flight tests with the energy absorber, the interval of operation of the unit was about 0.20 sec for flight 10 and about 0.125 sec for flight 11. In each flight test, the system was activated when the riser tension reached about 13 345 N (3000 lbf). During flight test 11, the shorter time interval of absorber effectiveness is probably accounted for by the higher energy input as exemplified by the resulting maximum load which was 46 085 N (10 360 lbf) or 70 percent higher than the 27 025-N (6075 lbf) opening load in flight test 10. During flight test 11, the cross parachute canopy shape was distorted. This distortion was probably due to permanent elongation of some suspension lines by the opening load which was 7 percent greater than the maximum design load of 43 150 N (9700 lbf) for this parachute as listed in table I. A result of the shape distortion was an oscillation and coning motion at an average angle off vertical of 17.8°.

Performance data (table III) for the cross parachute of flight test 10 compare favorably with those of the previous cross parachute flight tests. For flight test 11, however, the performance was noticeably affected by the canopy shape distortion mentioned earlier. The average $C_{D,o}$ of 0.83 is substantially higher than the range of average $C_{D,o}$ from 0.58 to 0.76 as established by the previous four flight tests of the cross parachute. The average $(C_{D,o})_{eff}$ of 0.90 was also substantially greater than the previously established range from 0.70 to 0.77. The L/D of 0.23 is not excessive and can be explained by the fact that the primary instability was coning which resulted in an average angle off vertical of 17.8^{o}.

CONCLUDING REMARKS

After an evaluation of data from 11 flight tests of the cross, modified ringsail, and disk-gap-band parachutes, it was determined that the deployment and inflation characteristics of the parachutes, up to the time of maximum opening load, were similar to those obtained in previous high-altitude flight tests. However, the maximum opening load encountered by the cross parachute under similar test conditions varied from 27 025 N (6075 lbf) to 46 085 N (10 360 lbf). After the instant of maximum opening load, some of the parachutes exhibited significant overinflation or shape distortion due to the airflow in the wake overtaking the rapidly decelerating canopy. These effects were very pronounced during the modified ringsail and disk-gap-band parachute tests; however, they were hardly noticeable during the cross parachute tests. For steady-state descent conditions, the drag and stability performance of the parachutes were similar to results obtained from previous high-altitude flight tests, with the exception of the modified ringsail which exhibited a higher effective drag coefficient at the lower test altitude.

Several additional objectives of these tests were met in that the method of instrumenting canopies to measure loads in structural members during deployment resulted in data useful for design and analysis purposes. The changes in the mortar deployment system proved to be satisfactory for these flight tests. Also, a method of retaining the parachute deployment bag and the mortar lid at the parachute apex was developed with no adverse effects on the parachute performance. The parachutes did not interfere with the payload after ground impact on any of the flight tests. In the flight tests of the energy absorber, the system deployed, activated, and operated as planned although the amount of energy absorbing material available was insufficient to maintain load attenuation for a long enough period of time to reduce the maximum parachute opening loads.

Langley Research Center,
National Aeronautics and Space Administration,
Hampton, Va., April 14, 1971.

REFERENCES

1. Murrow, Harold N.; and McFall, John C., Jr.: Some Test Results From the NASA Planetary Entry Parachute Program. J. Spacecraft Rockets, vol. 6, no. 5, May 1969, pp. 621-623.

2. Hoffman, Ira S.: Evaluation of a Parachute-Load-Distribution Measuring System During Low-Altitude Drop Tests. NASA TM X-1832, 1969.

3. Eckstrom, Clinton V.; and Preisser, John S.: Flight Test of a 40-Foot-Nominal-Diameter Disk-Gap-Band Parachute Deployed at a Mach Number of 2.72 and a Dynamic Pressure of 9.7 Pounds Per Square Foot. NASA TM X-1623, 1968.

4. Eckstrom, Clinton V.; and Preisser, John S.: Flight Test of a 30-Foot-Nominal-Diameter Disk-Gap-Band Parachute Deployed at a Mach Number of 1.56 and a Dynamic Pressure of 11.4 Pounds Per Square Foot. NASA TM X-1451, 1967.

5. Eckstrom, Clinton V.; Murrow, Harold N.; and Preisser, John S.: Flight Test of a 40-Foot-Nominal-Diameter Modified Ringsail Parachute Deployed at a Mach Number of 1.64 and a Dynamic Pressure of 9.1 Pounds Per Square Foot. NASA TM X-1484, 1967.

6. Preisser, John S.; and Eckstrom, Clinton V.: Flight Test of a 30-Foot-Nominal-Diameter Cross Parachute Deployed at a Mach Number of 1.57 and a Dynamic Pressure of 9.7 Pounds Per Square Foot. NASA TM X-1542, 1968.

7. Preisser, John S.; Eckstrom, Clinton V.; and Murrow, Harold N.: Flight Test of a 31.2-Foot-Diameter Modified Ringsail Parachute Deployed at a Mach Number of 1.39 and a Dynamic Pressure of 11.0 Pounds Per Square Foot. NASA TM X-1414, 1967.

8. Preisser, John S.; and Eckstrom, Clinton V.: Flight Test of a 40-Foot-Nominal-Diameter Disk-Gap-Band Parachute Deployed at a Mach Number of 1.91 and a Dynamic Pressure of 11.6 Pounds Per Square Foot. NASA TM X-1575, 1968.

9. Greene, George C.: Opening Distance of a Parachute. J. Spacecraft Rockets, vol. 7, no. 1, Jan. 1970, pp. 98-100.

10. Goble, Ross L.; and Councill, Earl L., Jr.: Ground and Flight Test Results of a Decelerator Towline Energy Absorber. AIAA Paper No. 70-1202, Sept. 1970.

11. Eckstrom, Clinton V.: Flight Test of a 40-Foot-Nominal-Diameter Disk-Gap-Band Parachute Deployed at a Mach Number of 3.31 and a Dynamic Pressure of 10.6 Pounds Per Square Foot. NASA TM X-1924, 1970.

TABLE I.- PARACHUTE DATA

Item	Flight test				
	1	2	3, 7, 9, 10, and 11	4 and 6	5 and 8
Parachute:					
Type	DGB	Modified ringsail	Cross	Modified ringsail	DGB
Nominal diameter, D_o, m	9.1	12.2	9.1	9.5	12.2
(ft)	(30)	(40)	(30)	(31.2)	(40)
Geometric porosity,[a] percent	15	15	0	15	12.5
Suspension lines (dacron):					
Number	24	36	36	24	32
Length, m	9.1	12.2	12.0	9.1	12.2
(ft)	(30)	(40)	(39.3)	(30)	(40)
Rated strength, N	2450	2450	2450	1560	2450
(lbf)	(550)	(550)	(550)	(350)	(550)
Canopy cloth (dacron):					
Unit weight, g/m^2	68	[b] 34	88	64	68
(ozm/yd^2)	2.0	(1.0)	(2.6)	(1.9)	(2.0)
Strength, N/cm	105	[b] 60	158	105	105
(lbf/in.)	(60)	(34)	(90)	(60)	(60)
Permeability, $m^3/min/m^2$ at 1.27-cm H_2O Δp	35	[b] 314	20	49	35
($ft^3/min/ft^2$ at 0.5-in. H_2O Δp)	(115)	(1030)	(67)	(162)	(115)
Parachute weight, kg	9.1	15.0	14.1	9.1	15.4
(lbm)	(20)	(33)	(31)	(20)	(34)
Maximum design load,[c] N	28 915	43 150	43 150	18 325	38 255
(lbf)	(6500)	(9700)	(9700)	(4120)	(8600)
Instrumented canopy	No	No	Yes	Yes	Yes

[a] Ratio of geometric open area within the boundaries of the canopy outer edges to the nominal surface area. By this definition the cross parachute has no geometric porosity.

[b] An exception was the first ring (next to the vent) which was fabricated of 64 g/m^2 (1.9 ozm/yd^2) material identical to that used in the 9.5-m (31.2 ft) ringsail parachute.

[c] Based on the suspension line rated strength and a design factor of 2.04.

TABLE II.- TEST CONDITIONS

Item	Flight test										
	1	2	3	4	5	6	7	8	9	10	11
Date	4-30-68	4-30-68	5-7-68	5-13-68	7-3-68	7-5-68	7-17-68	7-19-68	8-28-68	9-5-68	9-9-68
Drop number	0844F	0845F	0846F	0893F	1210F	1260F	1261F	1387F	1434F	1912F	1921F
Airplane type	C-130	C-130	T-33	T-33	T-33	T-33	T-33	T-33	T-33	T-33	T-33
Parachute type	DGB	Modified ringsail	Cross	Modified ringsail	DGB	Modified ringsail	Cross	DGB	Cross	Cross	Cross
Parachute diameter, m	9.1	12.2	9.1	9.5	12.2	9.5	9.1	12.2	9.1	9.1	9.1
(ft)	(30)	(40)	(30)	(31.2)	(40)	(31.2)	(30)	(40)	(30)	(30)	(30)
System weight, kg	295	295	177	172	179	179	179	272	272	272	272
(lbm)	(650)	(650)	(390)	(380)	(394)	(394)	(394)	(600)	(600)	(600)	(600)
Release velocity indicated airspeed, knots	120	150	150	150	150	120	150	150	150	150	150
Actual total velocity, m/sec	68.9	88.7	94.2	91.4	91.1	71.9	91.4	81.7	90.5	89.0	89.9
(ft/sec)	(226)	(291)	(309)	(300)	(299)	(236)	(300)	(268)	(297)	(292)	(295)
Release altitude, km	3.18	3.16	3.16	3.08	3.22	3.19	3.24	3.26	3.22	3.27	3.27
(ft)	(10 420)	(10 380)	(10 380)	(10 120)	(10 560)	(10 470)	(10 630)	(10 700)	(10 580)	(10 720)	(10 730)
Dynamic pressure at payload release, N/m^2	2075	3435	3875	3680	3540	2205	3610	2840	3500	3385	3445
(lbf/ft^2)	(43.3)	(71.7)	(80.9)	(76.9)	(73.9)	(46.1)	(75.4)	(59.3)	(73.1)	(70.7)	(71.9)
Mortar delay time, sec			3.238	3.182	3.335	3.129	3.105	[a] 14.240	3.227	3.158	3.146
Dynamic pressure at mortar firing, N/m^2			3845	3590	3560	2390	3520	8830	3600	3415	3690
(lbf/ft^2)			(80.3)	(75.0)	(74.4)	(50.0)	(73.5)	(184.4)	(75.2)	(71.3)	(77.1)
Surface wind velocity, m/sec	2.1	2.1	1.5	3.0	1.8	2.4	1.5	1.8	1.8	0.9	2.1
(ft/sec)	(7)	(7)	(5)	(10)	(6)	(8)	(5)	(6)	(6)	(3)	(7)
Surface wind direction, deg	030	030	110	210	190	230	120	010	280	310	300
Surface temperature, ^oC	30.0	30.0	29.9	18.7	33.5	30.0	28.5	35.8	32.6	30.8	35.0
(^oF)	(86.0)	(86.0)	(85.8)	(65.7)	(92.3)	(86.0)	(83.3)	(96.4)	(90.7)	(87.4)	(95.0)
Payload release time, hr:min	10:05	10:18	12:56	08:29	08:18	08:29	07:56	11:56	08:55	08:43	08:53
Rawinsonde release time, hr:min	10:55	10:55	13:00	08:31	10:05	08:25	08:15	Unknown	08:54	08:50	08:50

[a] The nominal timer setting was 3 sec; however, improper cycling of the timer resulted in the 14-sec delay which allowed the test payload to free fall to a velocity and dynamic pressure greater than the parachute could withstand.

TABLE III.- PERFORMANCE DATA

Item	Flight test										
	1	2	3	4	5	6	7	8	9	10	11
Date	4-30-68	4-30-68	5-7-68	5-13-68	7-3-68	7-5-68	7-17-68	7-19-68	8-28-68	9-5-68	9-9-68
Parachute type	DGB	Modified ringsail	Cross	Modified ringsail	DGB	Modified ringsail	Cross	DGB	Cross	Cross	Cross
Parachute diameter, m	9.1	12.2	9.1	9.5	12.2	9.5	9.1	12.2	9.1	9.1	9.1
(ft)	(30)	(40)	(30)	(31.2)	(40)	(31.2)	(30)	(40)	(30)	(30)	(30)
Event times:[a]											
Line stretch, sec			0.42	0.31	0.46	0.39	0.48	0.45	0.47	0.48	0.52
Maximum load, sec			1.10	1.28	1.35	1.34	1.18	0.93		1.23	1.27
First canopy opening, sec	2.6	(c)	3.0	1.4	1.9	(b)	1.8	(b)	1.9	2.0	1.8
Stable canopy inflation, sec	8.8	(c)	4.8	6.0	6.8	(b)	3.1	(b)	3.5	2.8	3.6
Ground impact, sec	232	104	356	342	413	59	365	38	302	310	327
Snatch force load, N	Not measured		5340	6230	7120	5785	5115	10 675		5785	5340
(lbf)			(1200)	(1400)	(1600)	(1300)	(1150)	(2400)		(1300)	(1200)
Maximum opening load, N	26 910	11 120	16 015	24 910	19 570	22 240	22 685	28 025	[d]31 140	27 025	46 085
(lbf)	(6050)	(2500)	(3600)	(5600)	(4400)	(5000)	(5100)	(6300)	(≈7000)	(6075)	(10 360)
Opening distance, m			105	75	72		75		62	93	69
(ft)			(345)	(246)	(236)		(246)		(204)	(305)	(226)
Average $C_{D,o}$	0.46	0.05	0.69	0.55	[e]0.37	0.015	0.58	0.014	0.74	0.76	0.83
Average L/D	0.14		0.26	0.36	[e]0.57		0.39		0.14	0.16	0.23
Average angle off vertical, deg	12.7		2.2	6.8	6.8		4.4		1.8	5.6	17.8
Adjusted average rate of descent, m/sec	12.3	27.9	7.8	7.8	6.7	51.4	7.7	52.3	9.3	9.2	8.6
(ft/sec)	(40.3)	(91.5)	(25.7)	(25.7)	(21.9)	(168.5)	(25.4)	(171.7)	(30.5)	(30.3)	(28.1)
Average $(C_{D,o})_{eff}$	0.48		0.70	0.63	0.55		0.72		0.76	0.77	0.90
Comments	Good test	Failed to open	Good test	Good test	Good test	Parachute failure	Good test	Parachute failure[f]	Good test	Good test	Good test
Damage	None	None	Minor[g]	Minor[h]	Lost bag and lid	Major; lost bag and lid[i]	Lost lid	Major; lost lid[j]	Lost bag and lid	Minor	Lost lid

[a] For flight tests 1 and 2, times listed are from release from airplane; for flight tests 3 to 11, times are from mortar firing.

[b] Parachutes failed during opening.

[c] Did not open fully.

[d] Estimated total load based on measured load in 3 of 36 suspension lines.

[e] These values are questionable due to lack of appropriate wind data for calculations.

[f] Improper mortar delay time resulted in greater velocity and dynamic pressure than the parachute could withstand.

[g] Lost wood spacer block from deployment bag.

[h] One suspension line broken and other minor canopy damage.

[i] Broke 15 of 24 suspension lines plus extensive canopy damage.

[j] Broke 12 of 32 suspension lines plus extensive canopy damage.

Legend	◇ Master Control Center ○ Cinetheodolite station A - Askania C - Contraves

Flight Test	Cinetheodolite station used A5 A6 A7 A8 C9 C10 C11
1	X X X
2	X X X
3	X X X
4	X X X
5	X X X
6	X X X
7	X X X
8	X X X
9	X X X
10	X X X
11	X X X

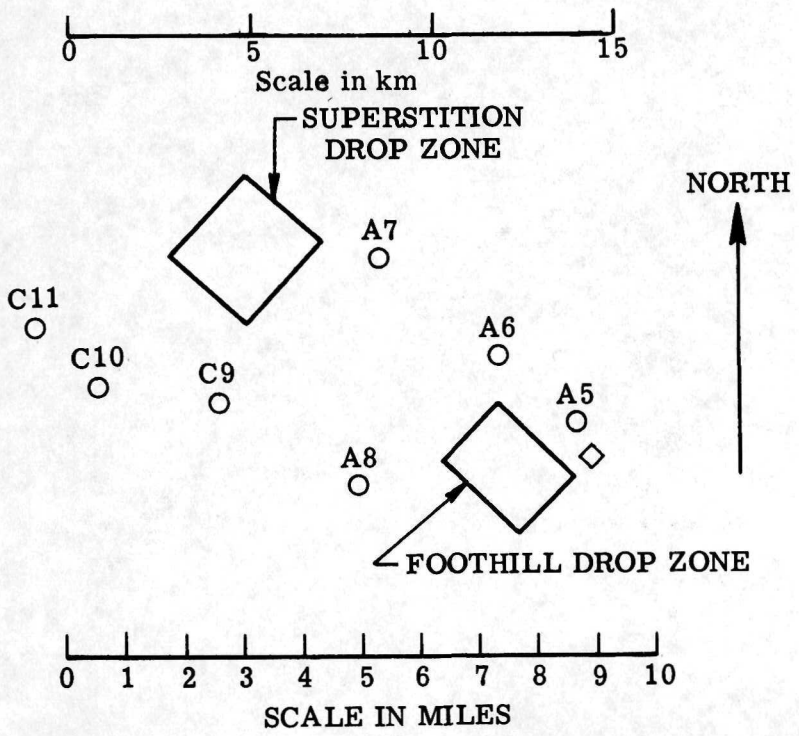

Figure 1.- Sketch showing the cinetheodolite station network used for various flight tests.

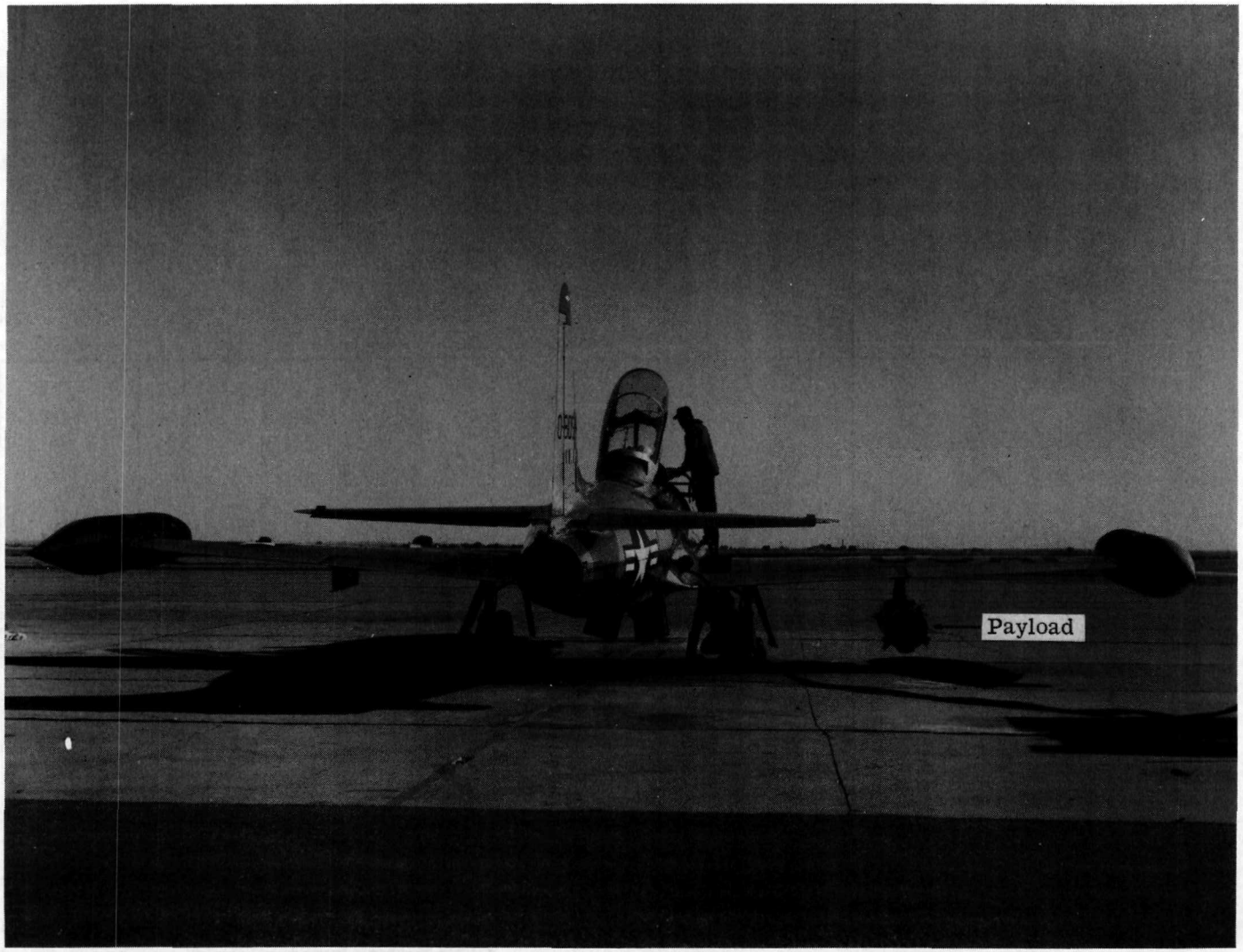

L-71-540

Figure 2.- T-33 airplane with payload. U.S. Navy photograph.

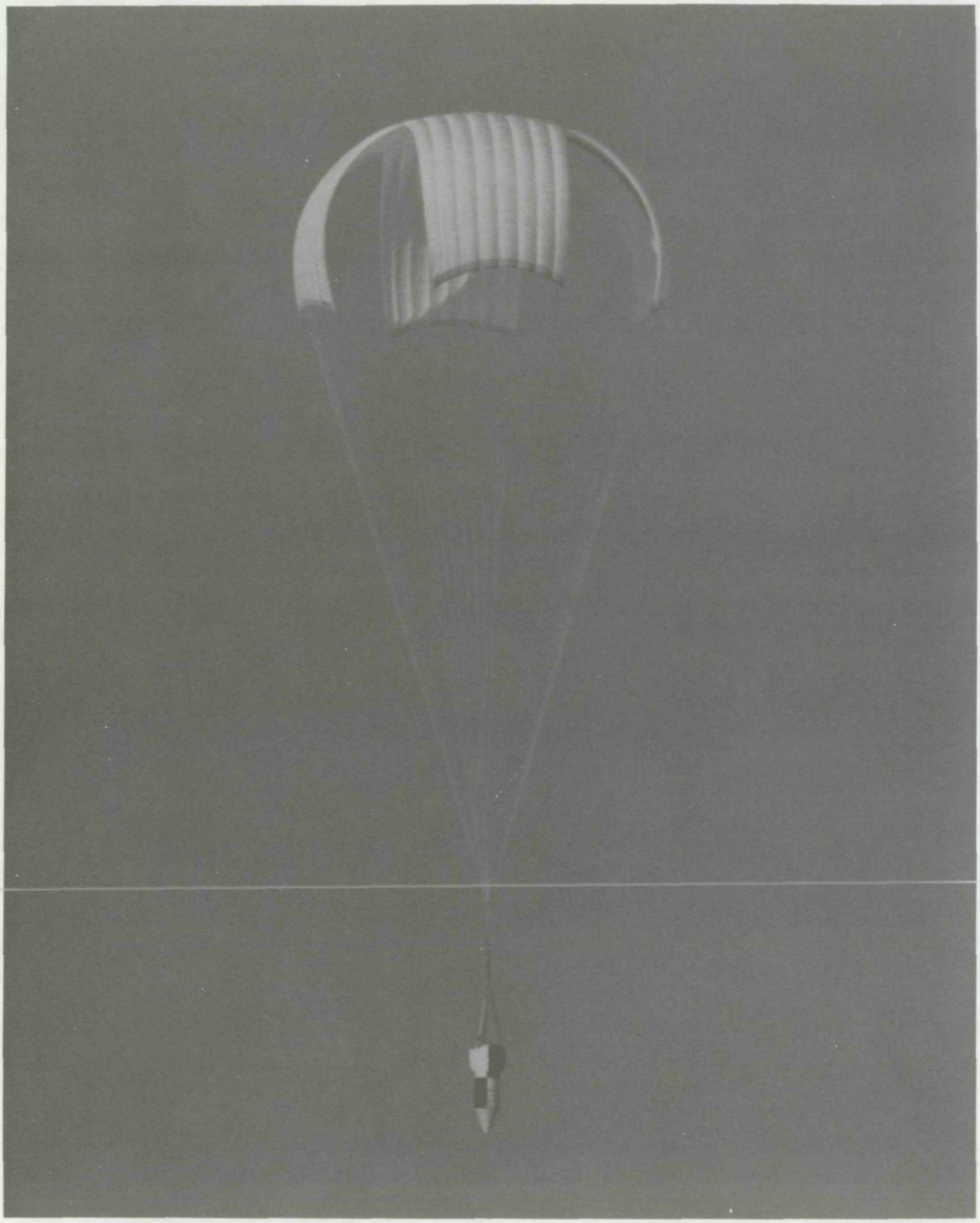

L-71-541

(a) Cross parachute with instrumented payload.

Figure 3.- Test parachute configurations. U.S. Navy photograph.

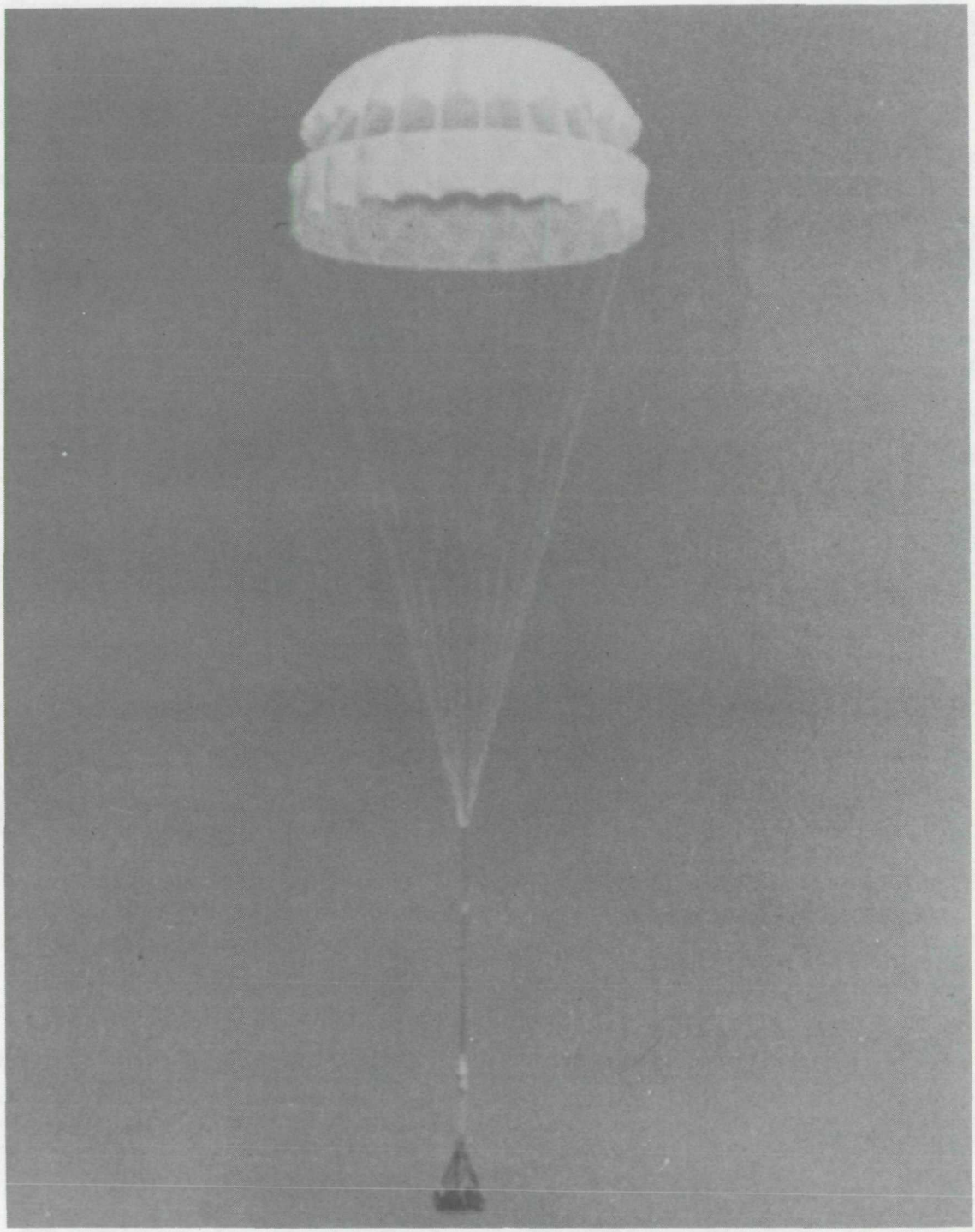

L-71-542

(b) Disk-gap-band parachute with inert payload on flight test 1.

Figure 3.- Continued.

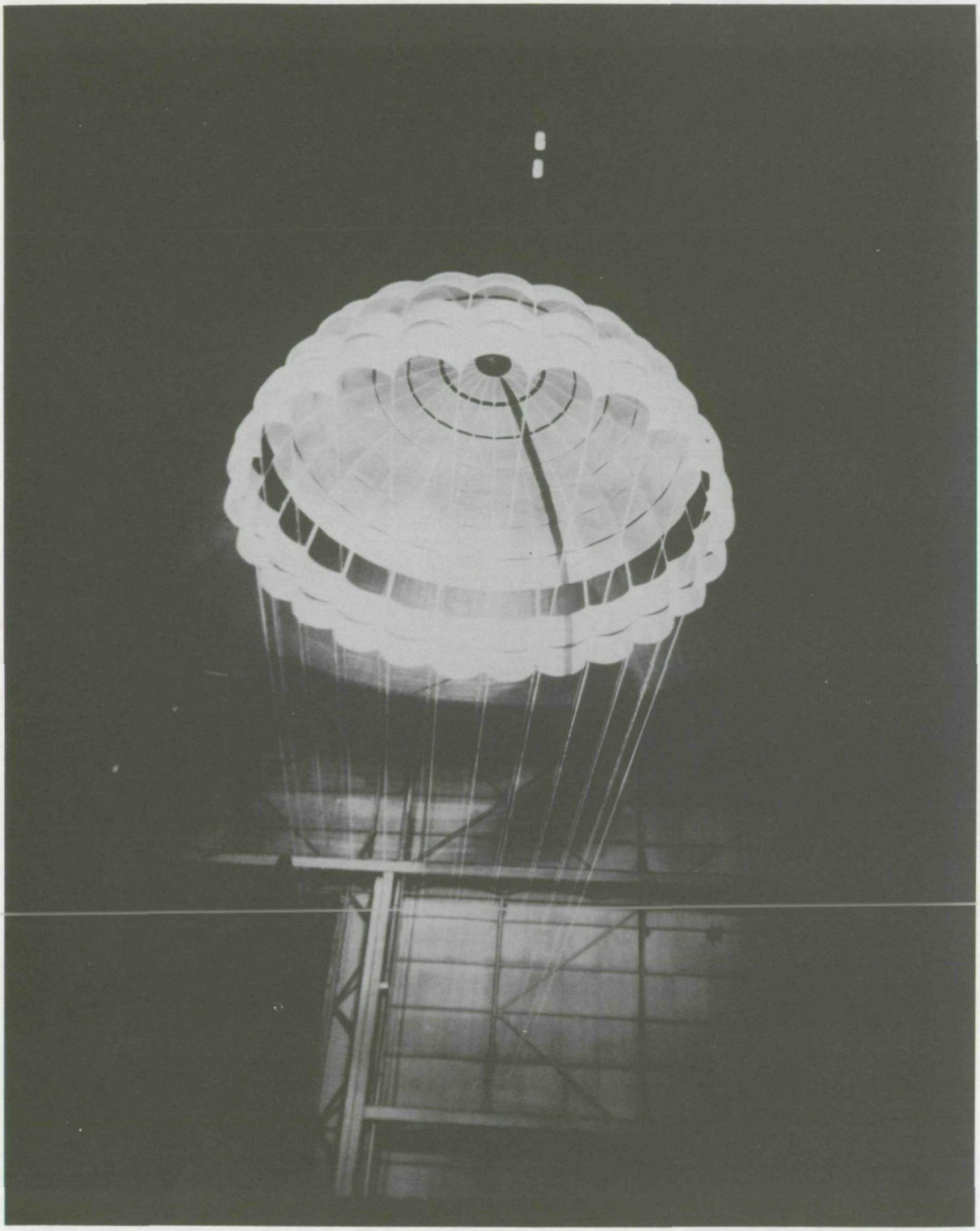

L-71-543

(c) 9.5-m-nominal-diameter (31.2 ft) modified ringsail parachute during wind-tunnel checkout.

Figure 3.- Concluded.

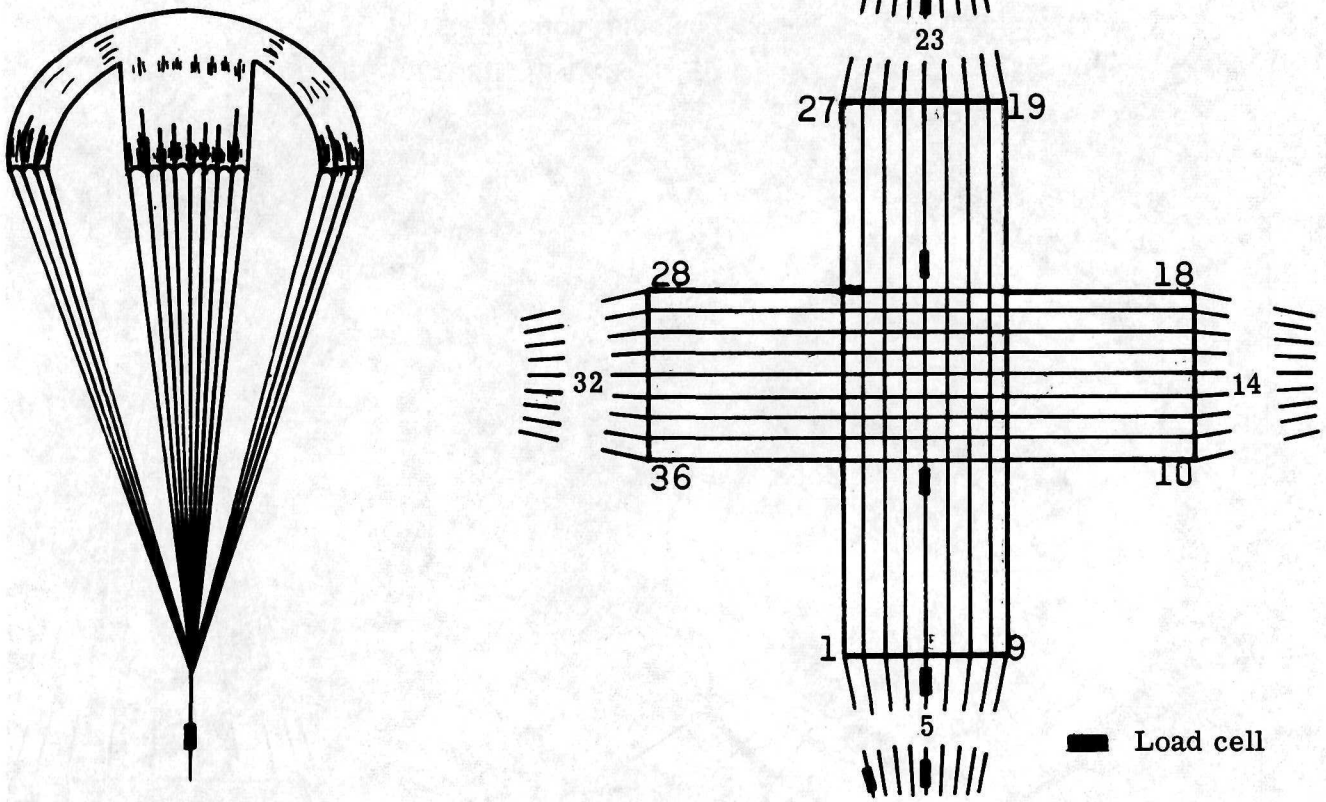

Figure 4.- Load cell locations in 9.1-m (30 ft) cross parachute. (Numbers identify suspension lines and canopy tapes.)

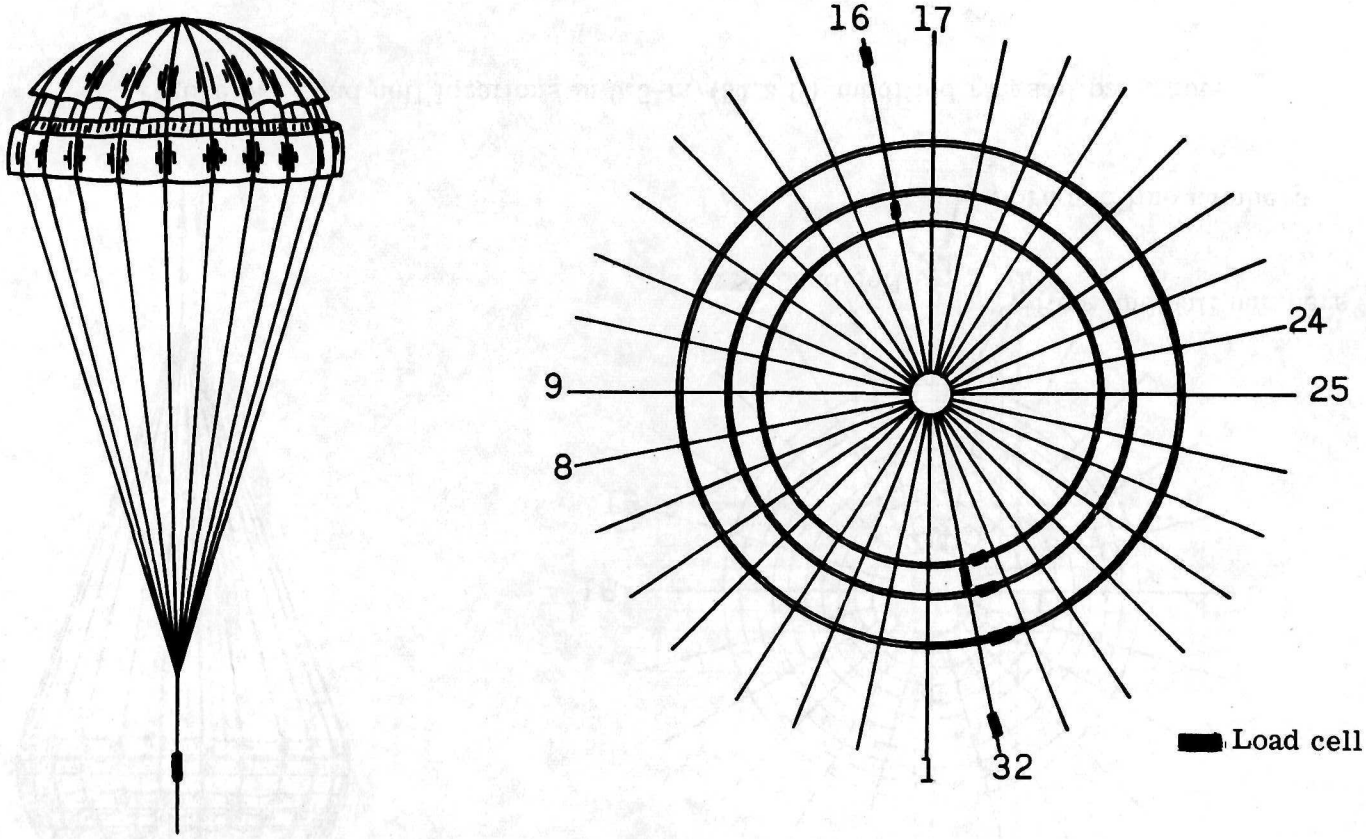

Figure 5.- Load cell locations in 12.2-m (40 ft) DGB parachute. (Numbers identify suspension lines and canopy tapes.)

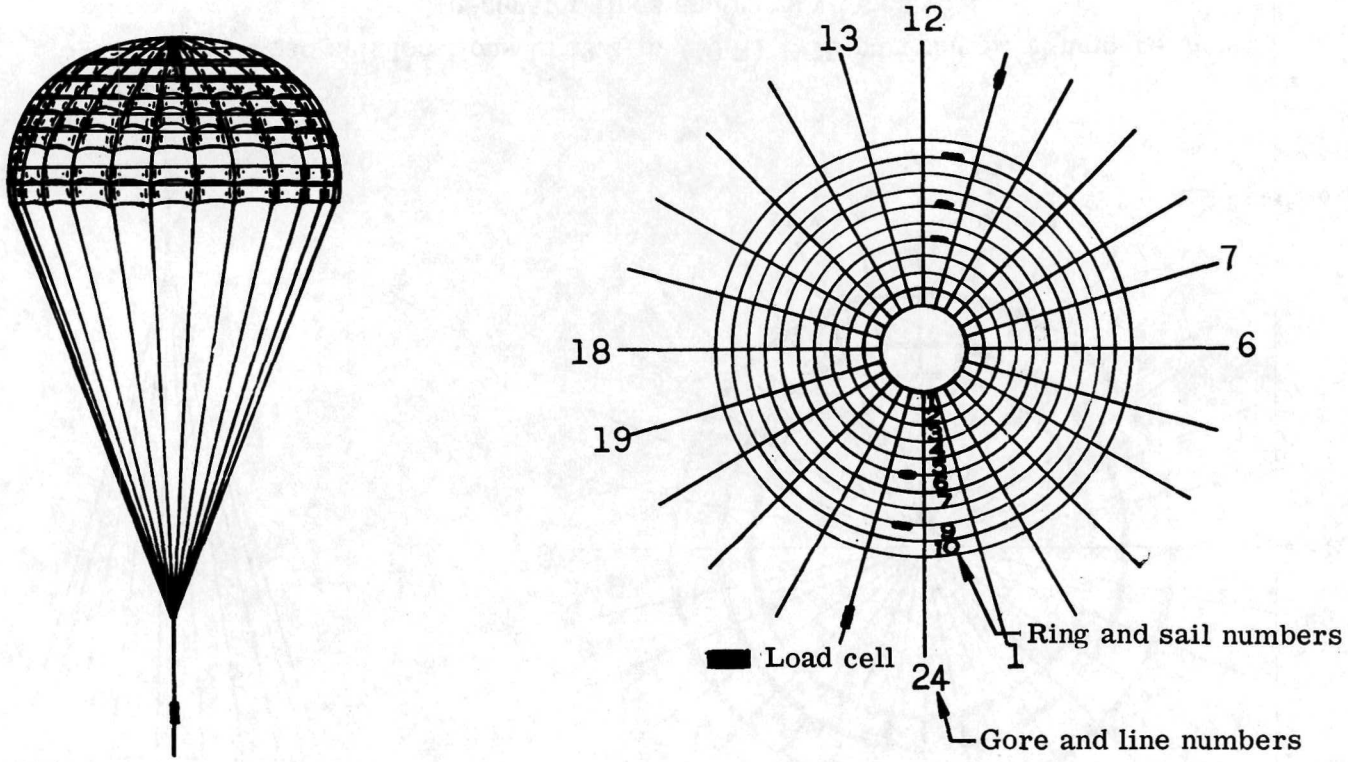

Figure 6.- Load cell locations in 9.5-m (31.2 ft) modified ringsail parachute.

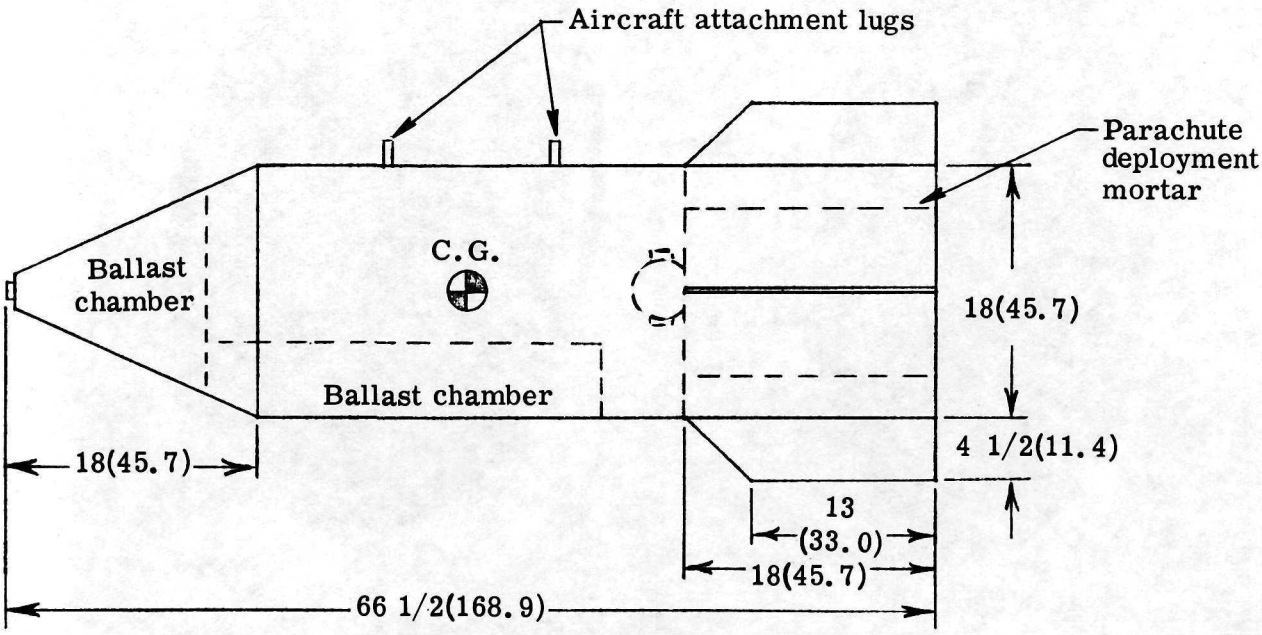

Figure 7.- Instrumented test vehicle. Dimensions are in inches (centimeters).

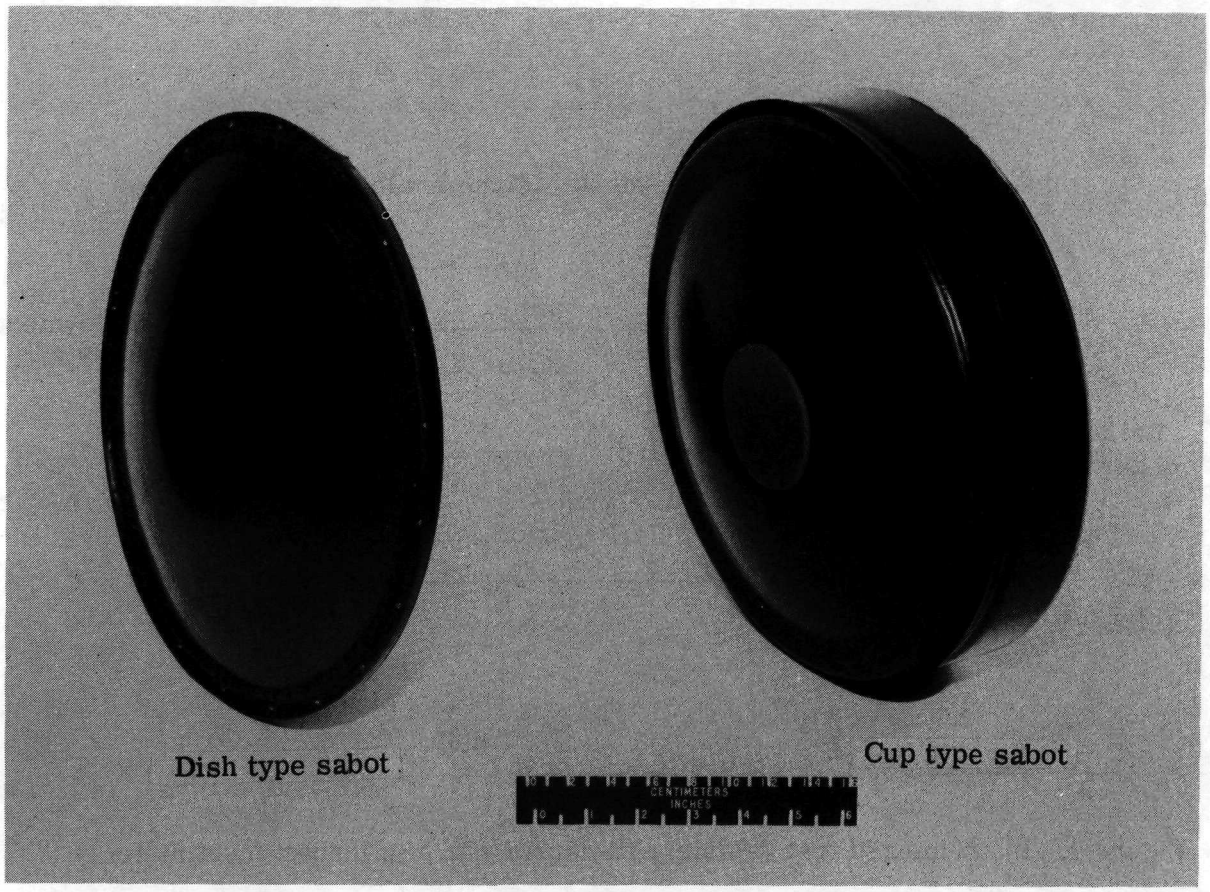

L-69-2059.1

Figure 8.- Mortar sabots.

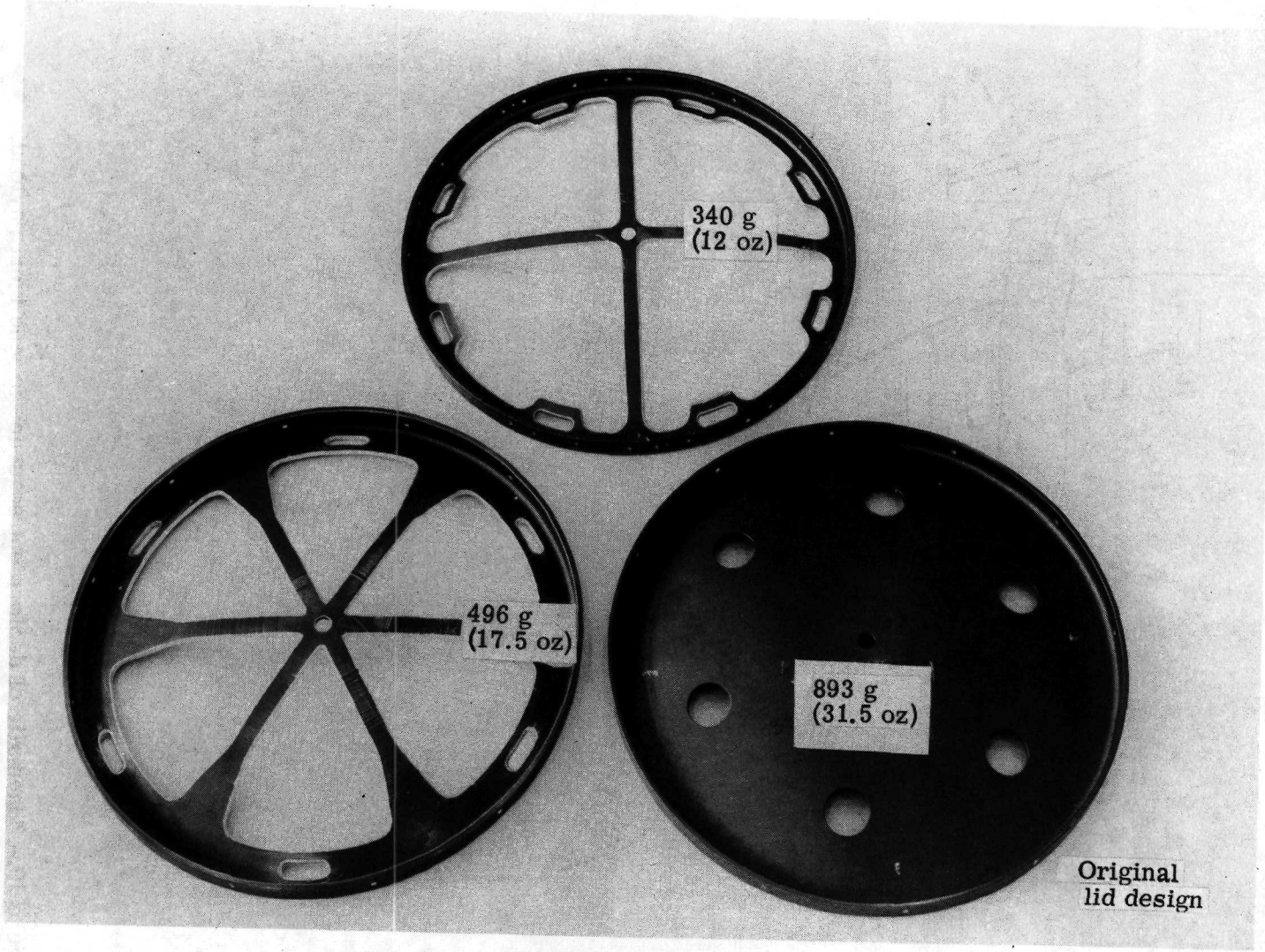

Figure 9.- Mortar lids.

L-69-1452.1

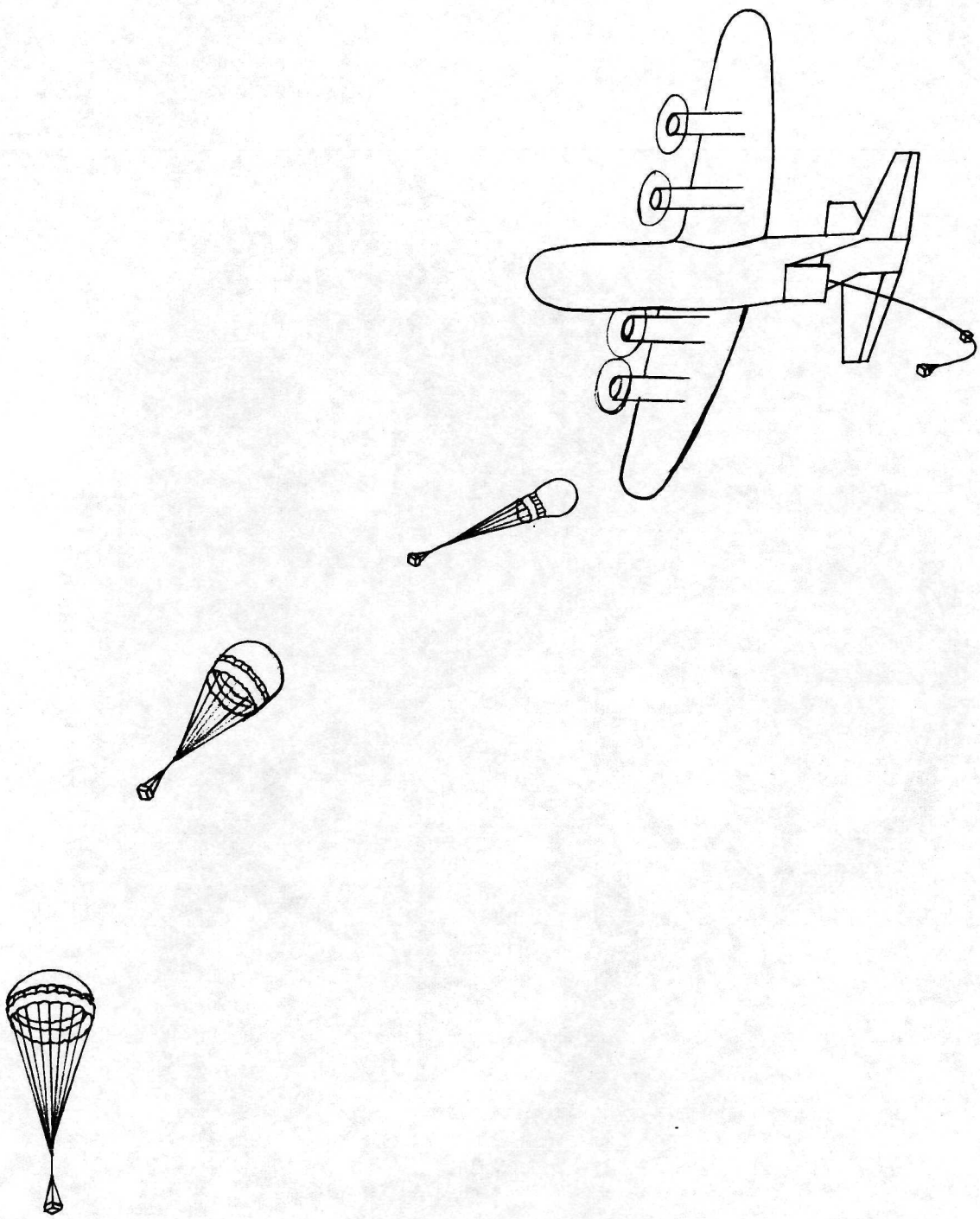

Figure 10.- Schematic of deployment sequence for the inert payload.

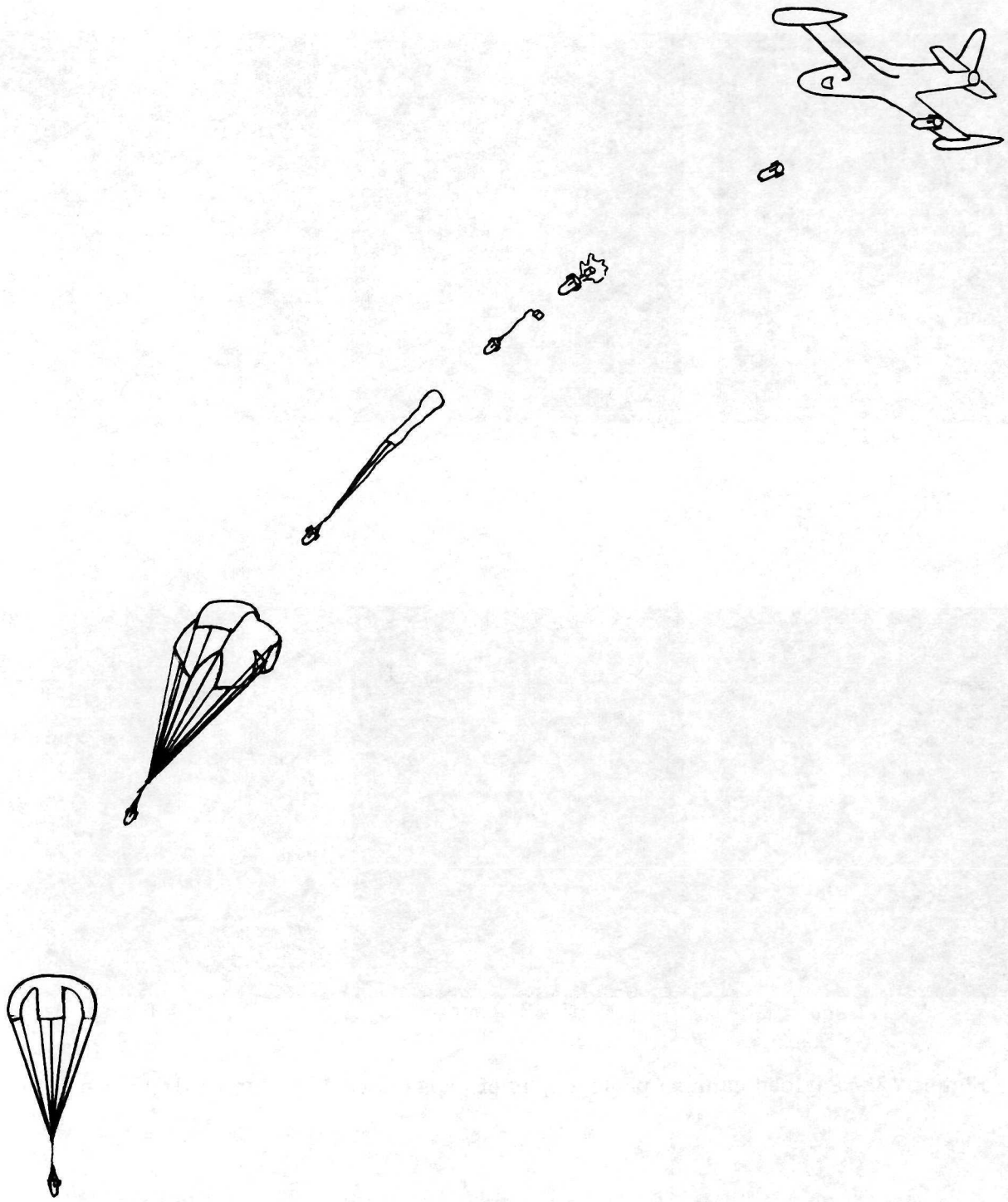

Figure 11.- Schematic of deployment sequence for the instrumented payload.

t' = 0.11 sec t' = 0.425 sec t' = 0.9 sec

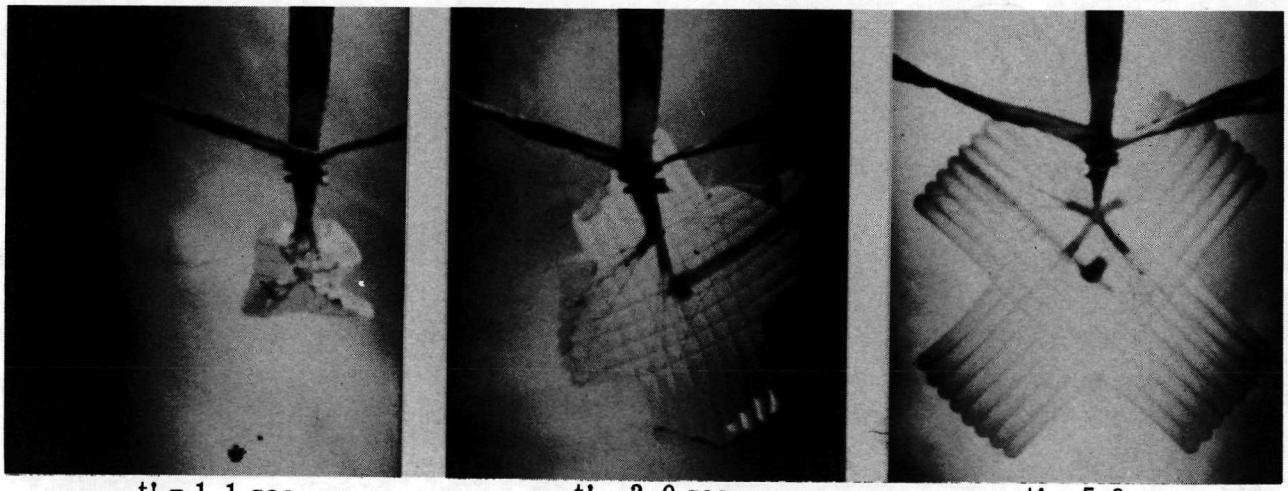

t' = 1.1 sec t' = 3.0 sec t' = 5.9 sec

L-71-544

Figure 12.- Payload camera photographs of cross parachute during flight test 3.

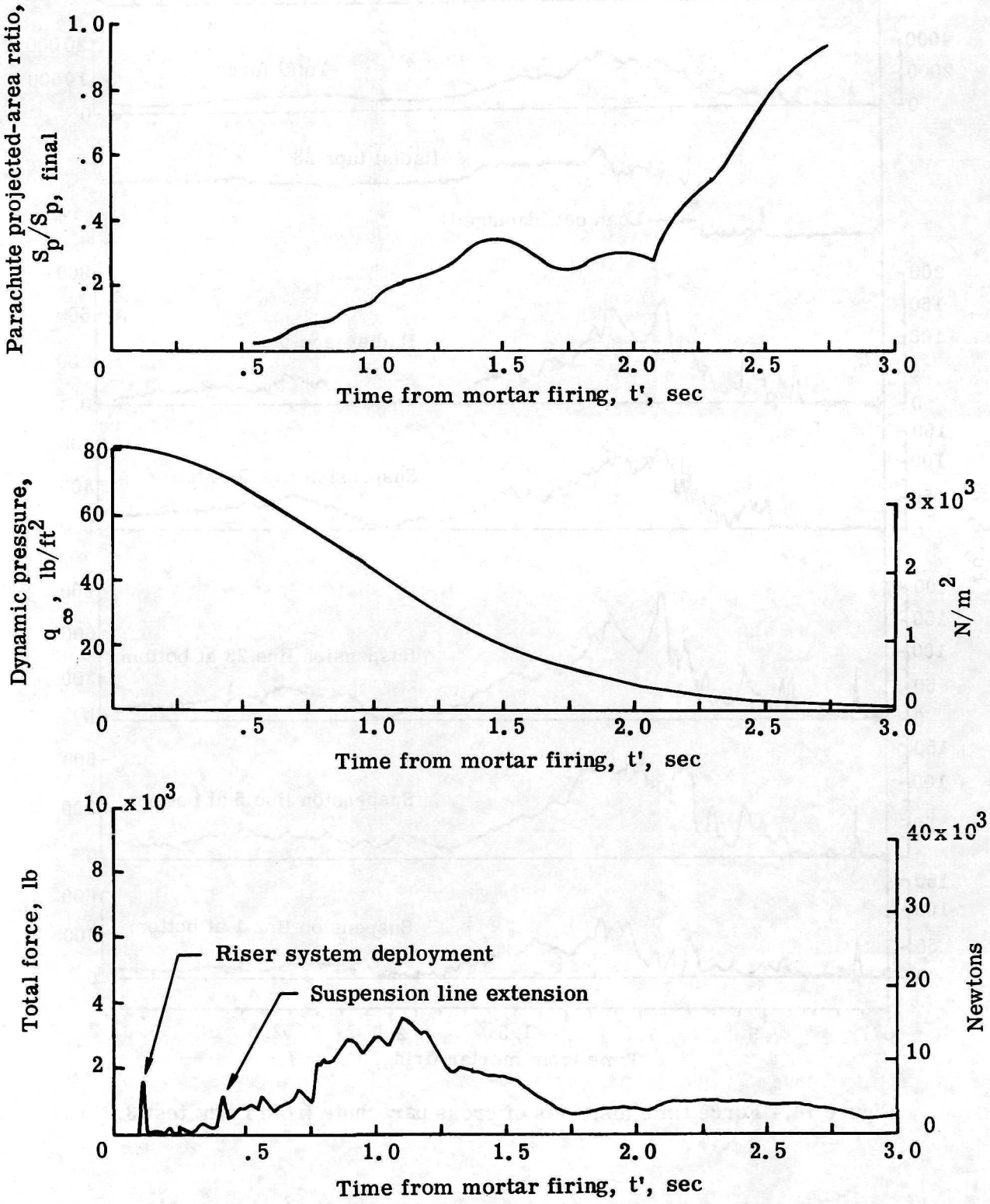

Figure 13.- Time history of the cross parachute projected-area ratio, dynamic pressure, and total force from flight test 3.

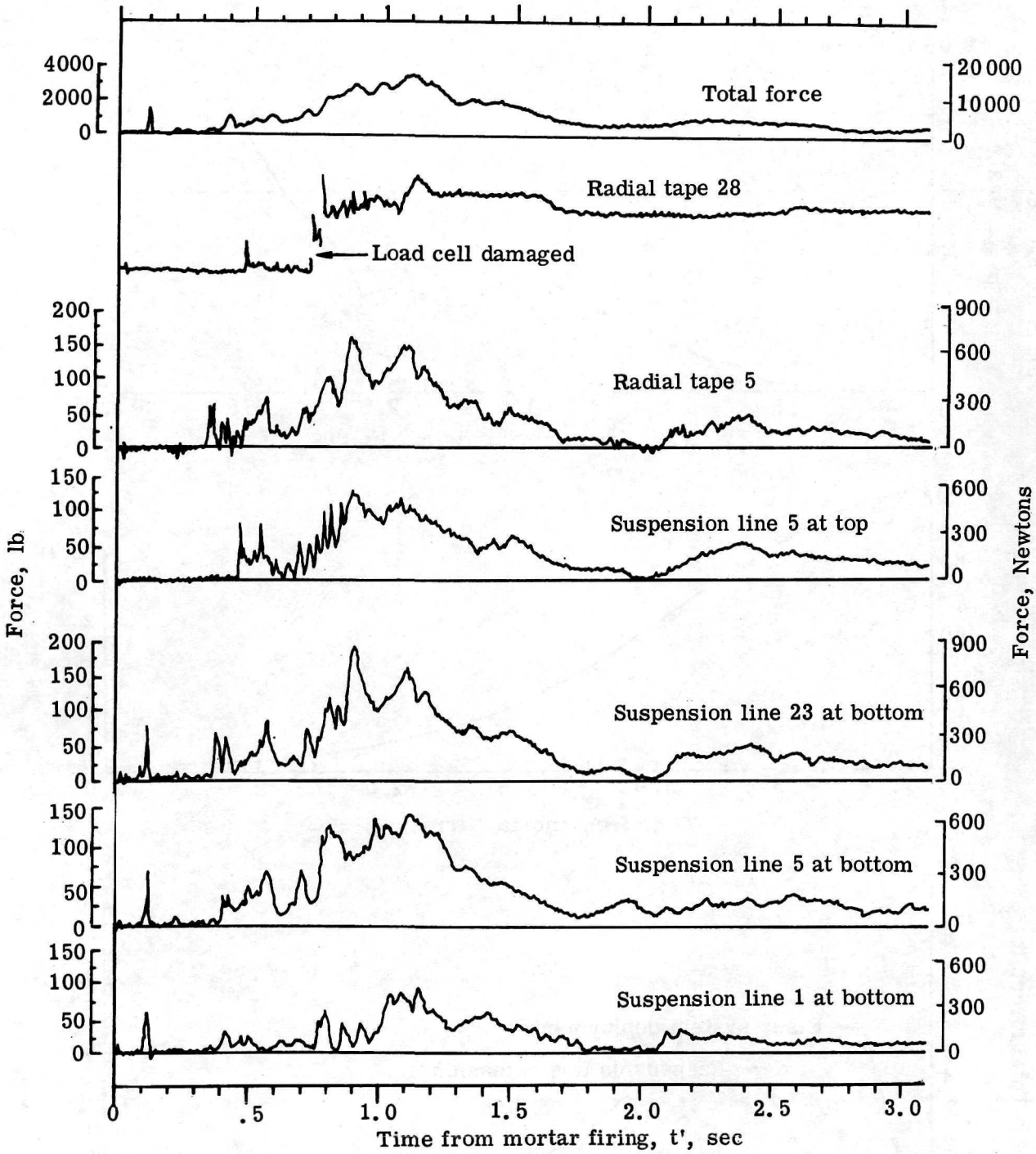

Figure 14.- Force time histories of cross parachute from flight test 3.

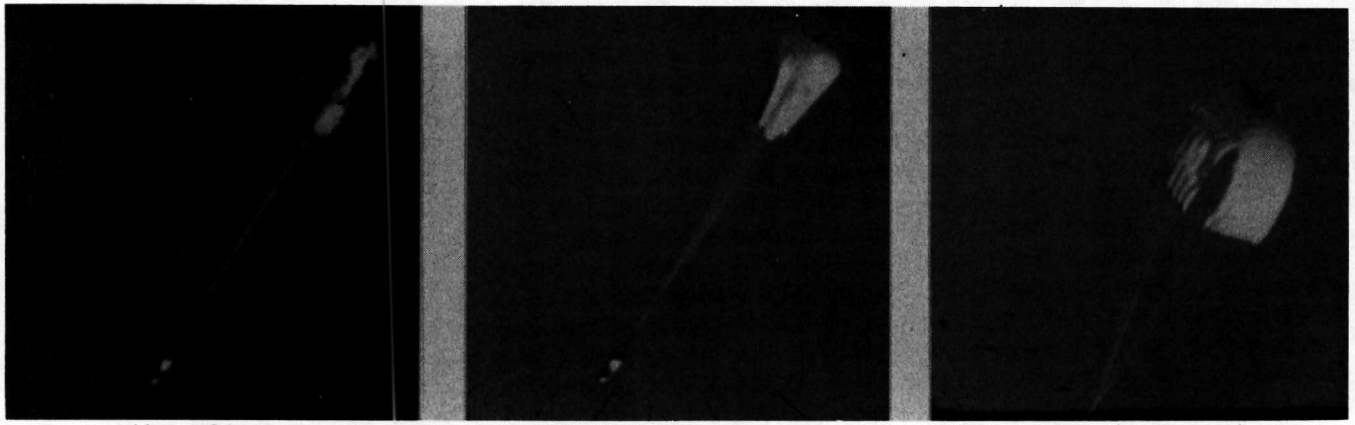

t' = .60 sec t' = .91 sec t' = 1.47 sec

Profile views of steady-state descent

L-71-545

Figure 15.- Ground-based camera photographs of cross parachute during flight test 7.

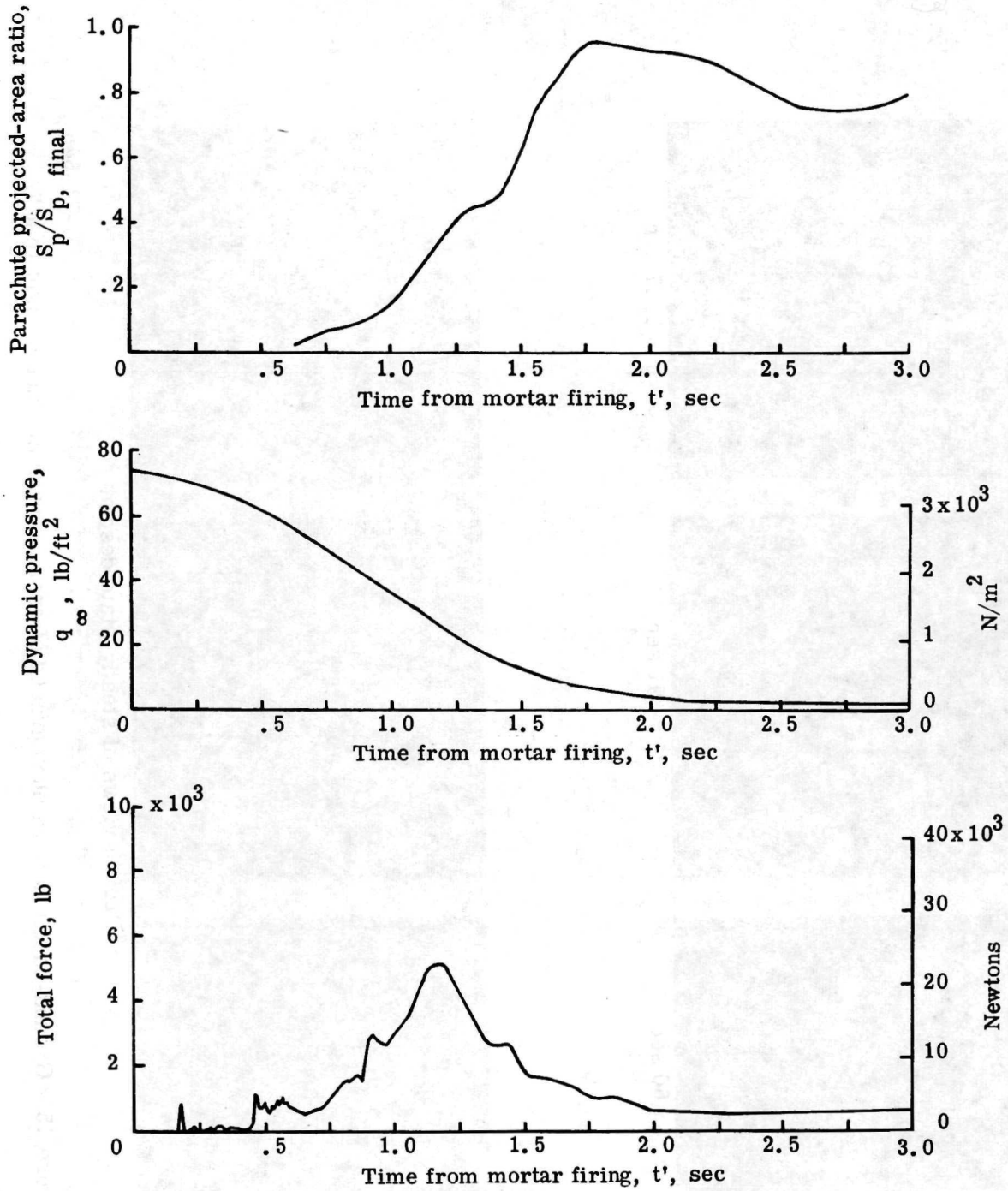

Figure 16.- Time history of the cross parachute projected-area ratio, dynamic pressure, and total force from flight test 7.

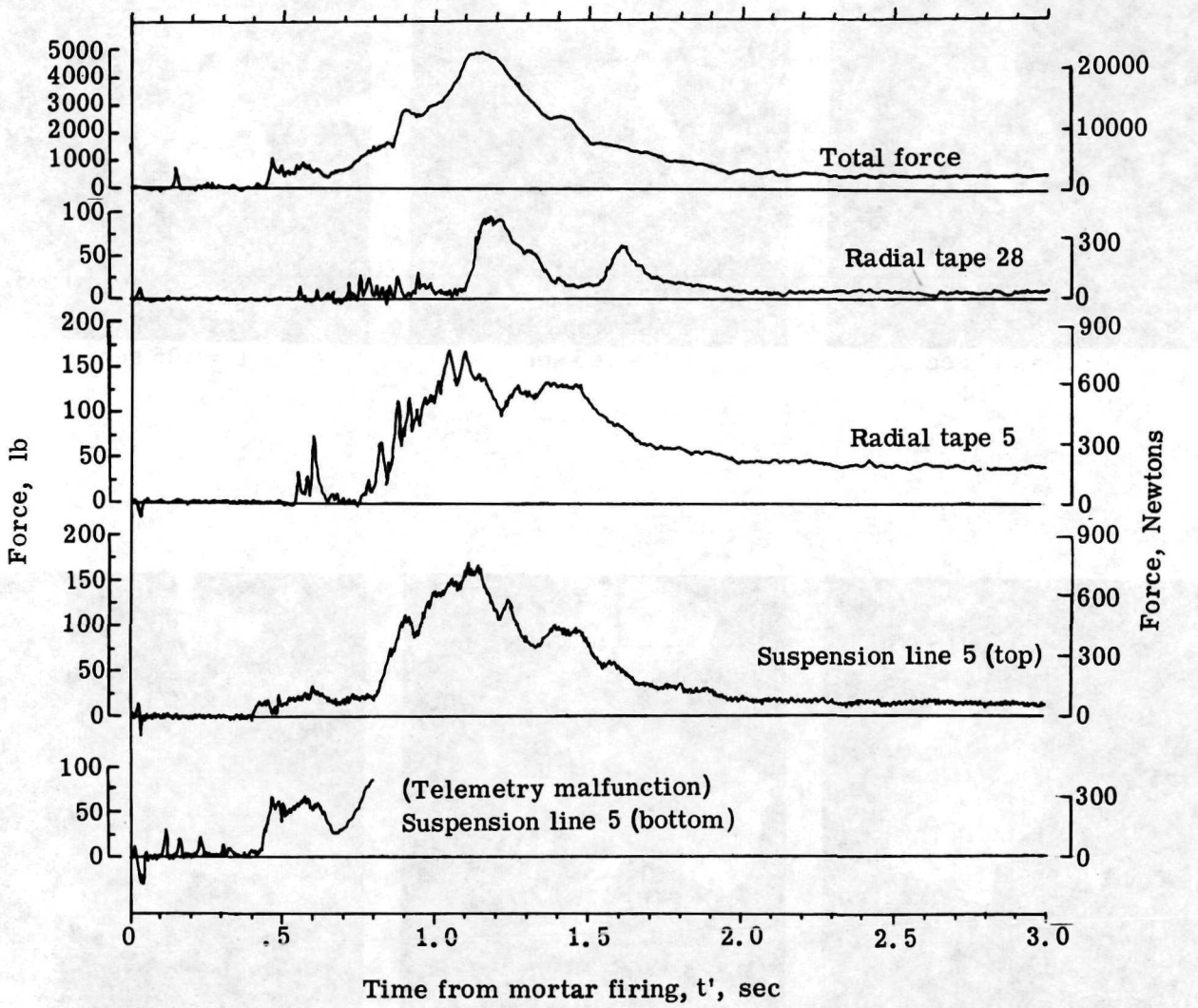

Figure 17.- Force time histories of cross parachute from flight test 7.

t' = .17 sec t' = .45 sec t' = .95 sec

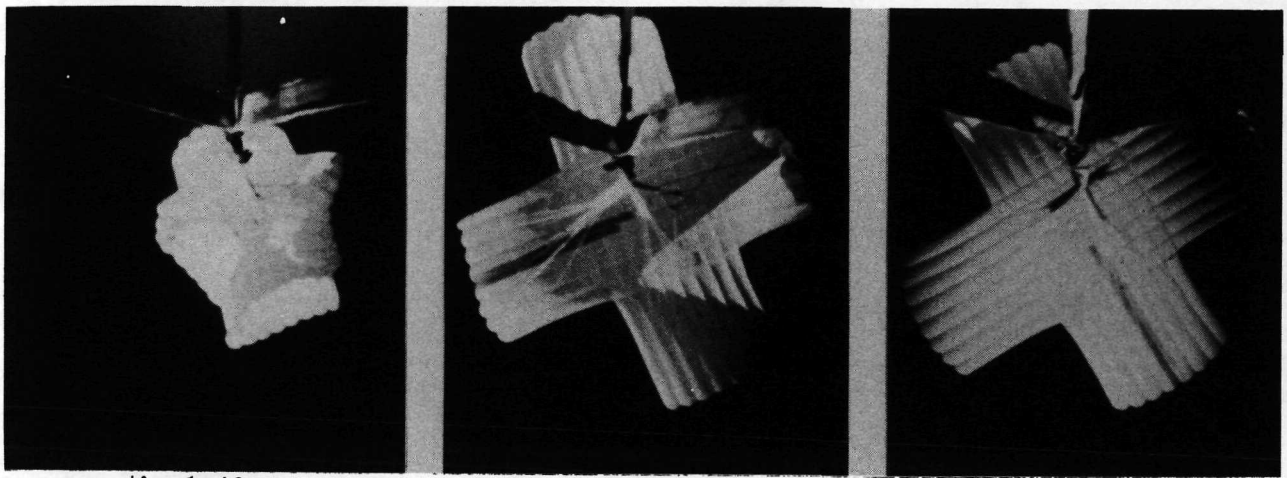

t' = 1.40 sec t' = 2.25 sec steady-state descent

L-71-546

Figure 18.- Payload camera photographs of cross parachute during flight test 9.

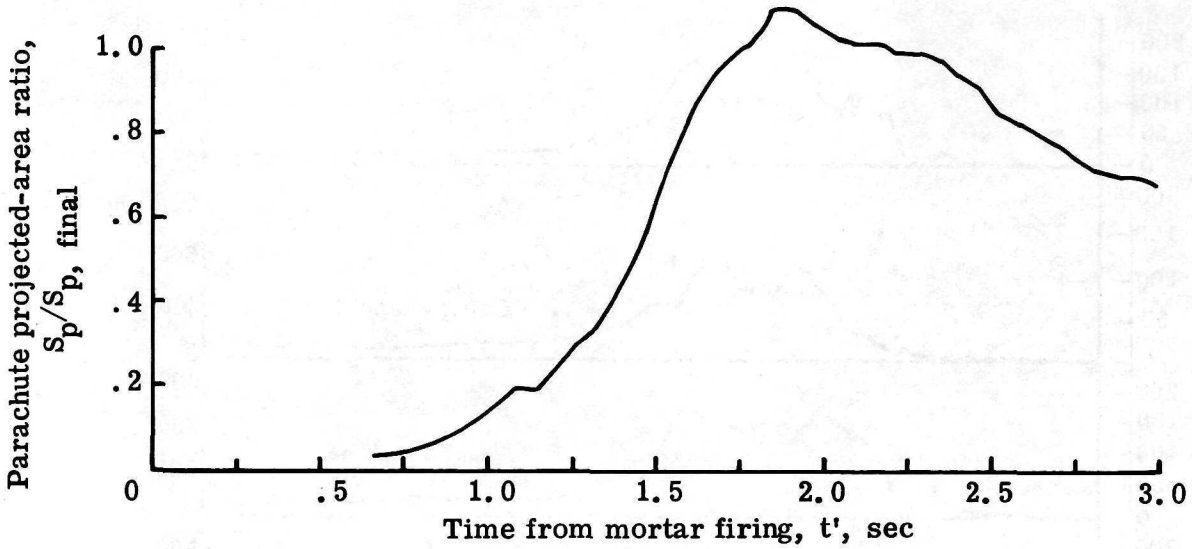

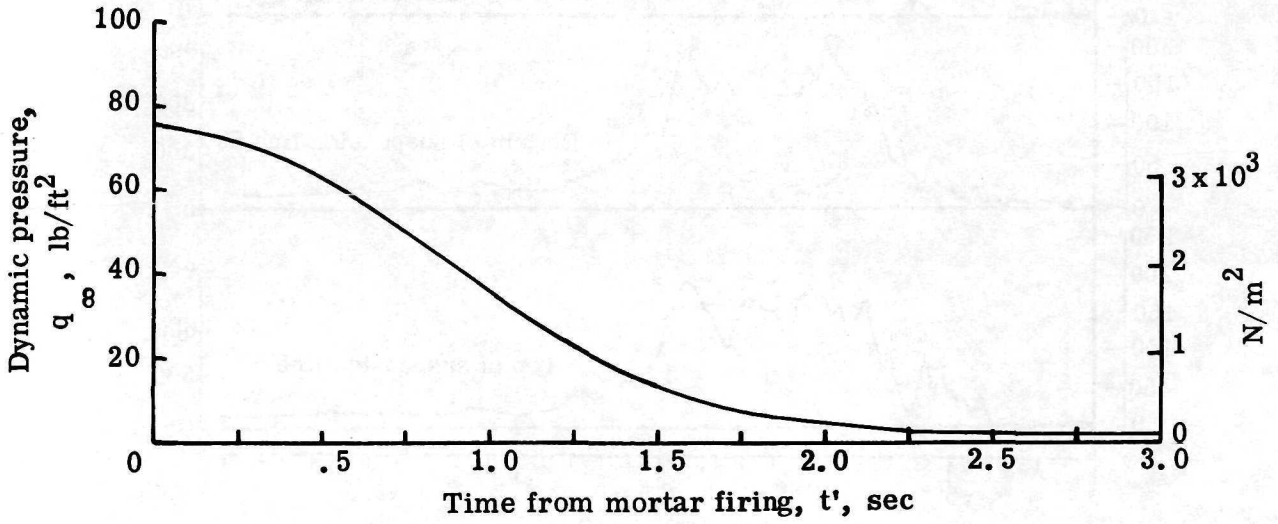

Figure 19.- Time history of the cross parachute projected-area ratio and dynamic pressure from flight test 9.

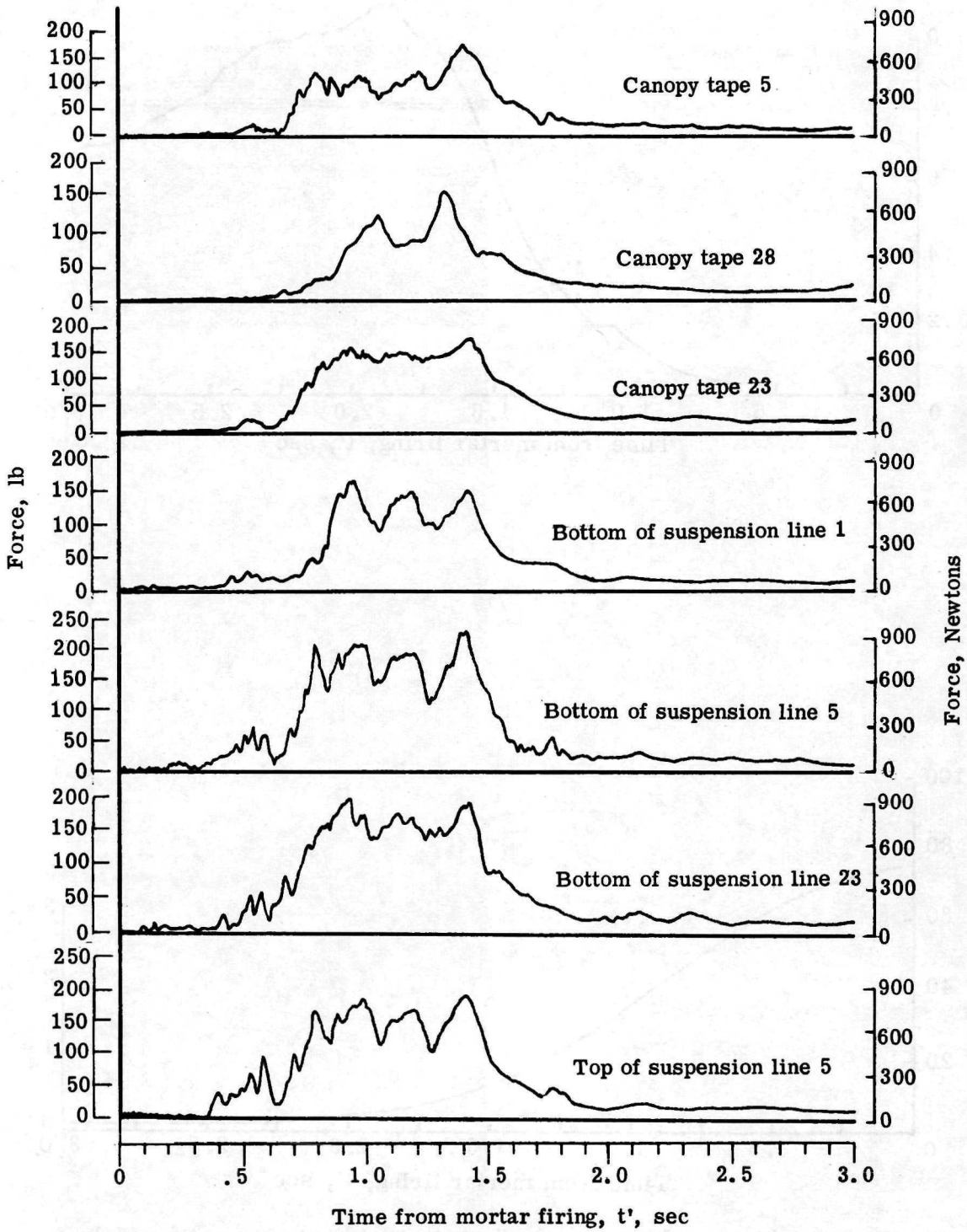

Figure 20.- Force time histories of cross parachute from flight test 9.

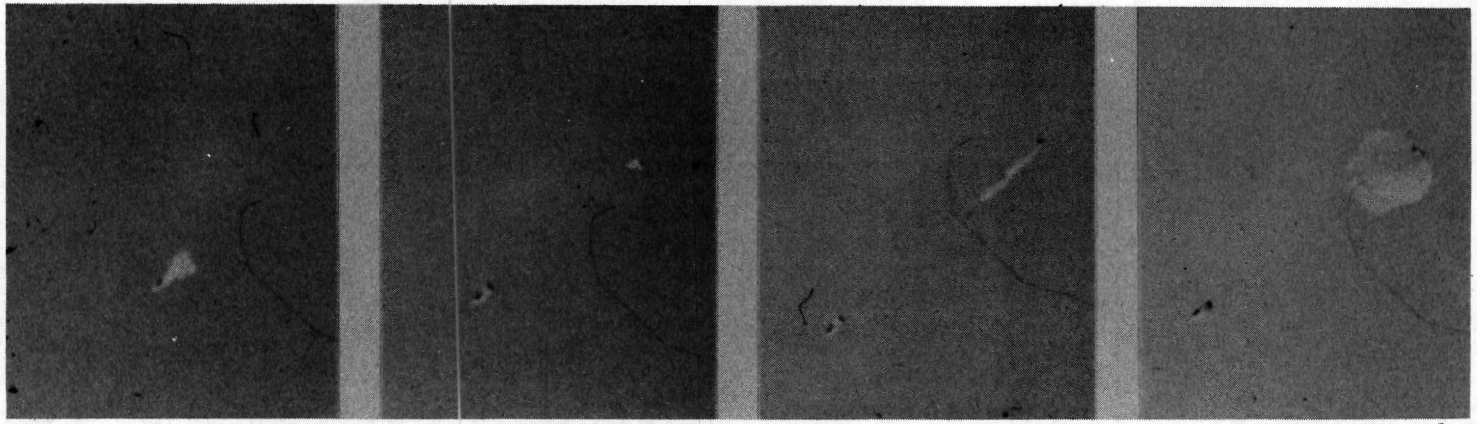

t' = .015 sec, mortar firing t' = .31 sec, line stretch t' = .44 sec, bag strip t' = 1.28 sec, max. load

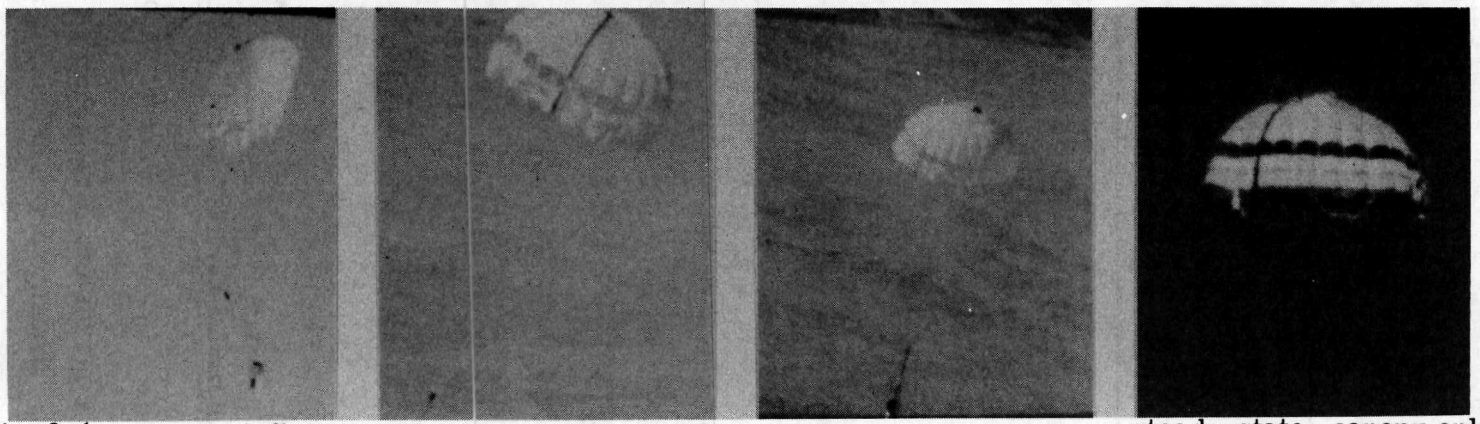

t' = 2.1 sec, overinflation steady-state descent steady-state descent steady-state, canopy only

L-71-547

Figure 21.- Ground-based camera photographs of modified ringsail parachute during flight test 4.

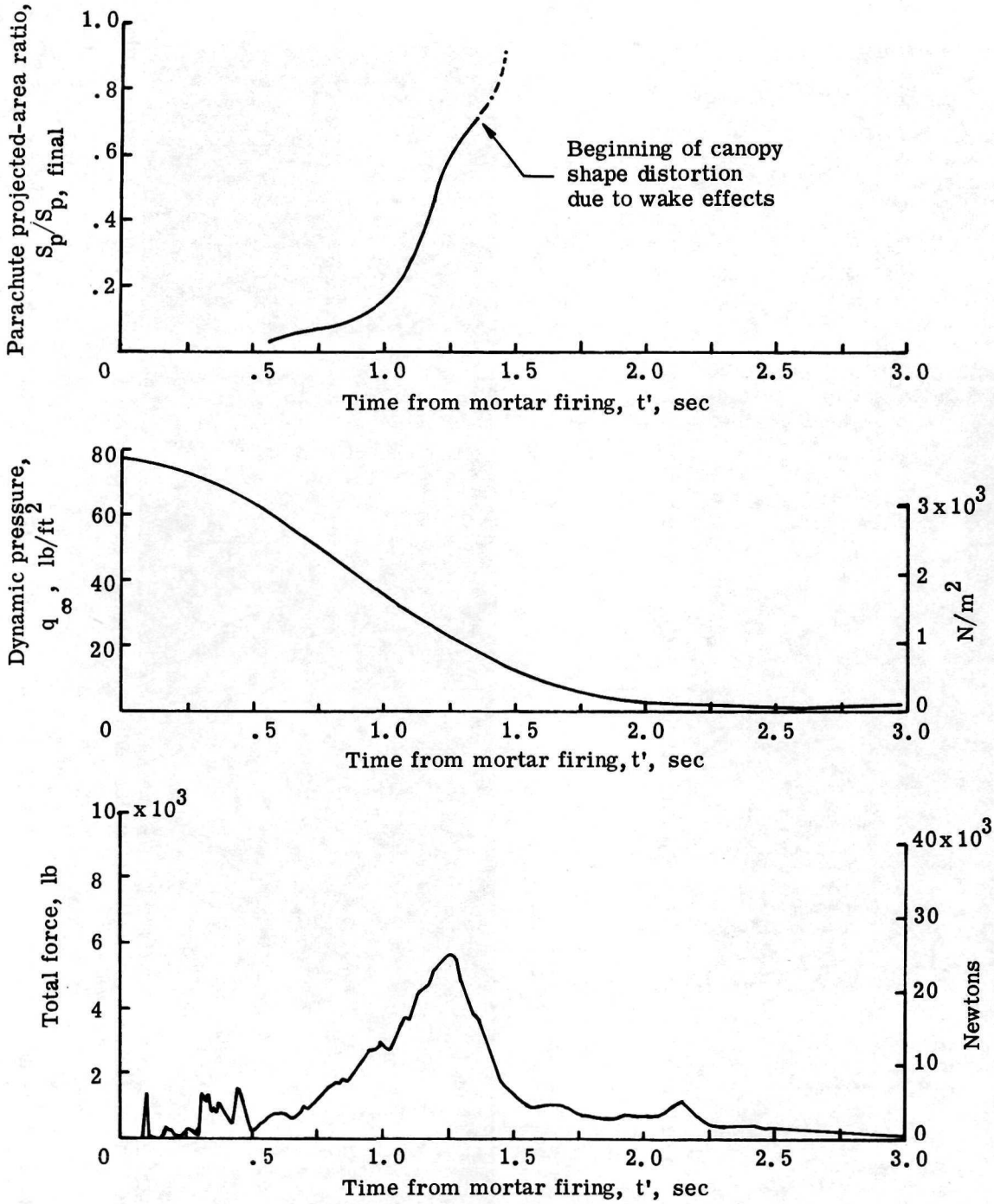

Figure 22.- Time history of the modified ringsail parachute projected-area ratio, dynamic pressure, and total force from flight test 4.

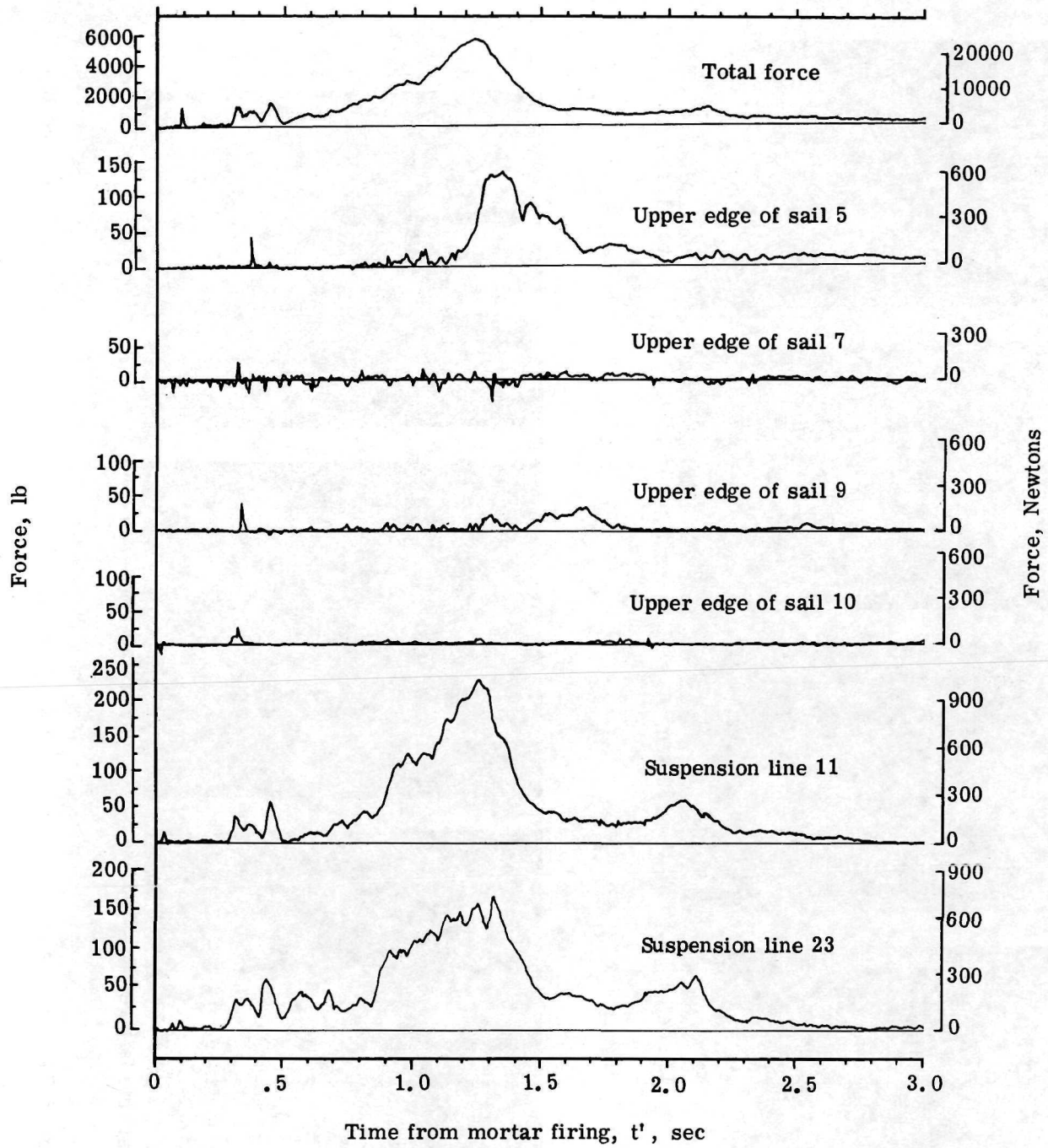

Figure 23.- Force time histories of modified ringsail parachute from flight test 4.

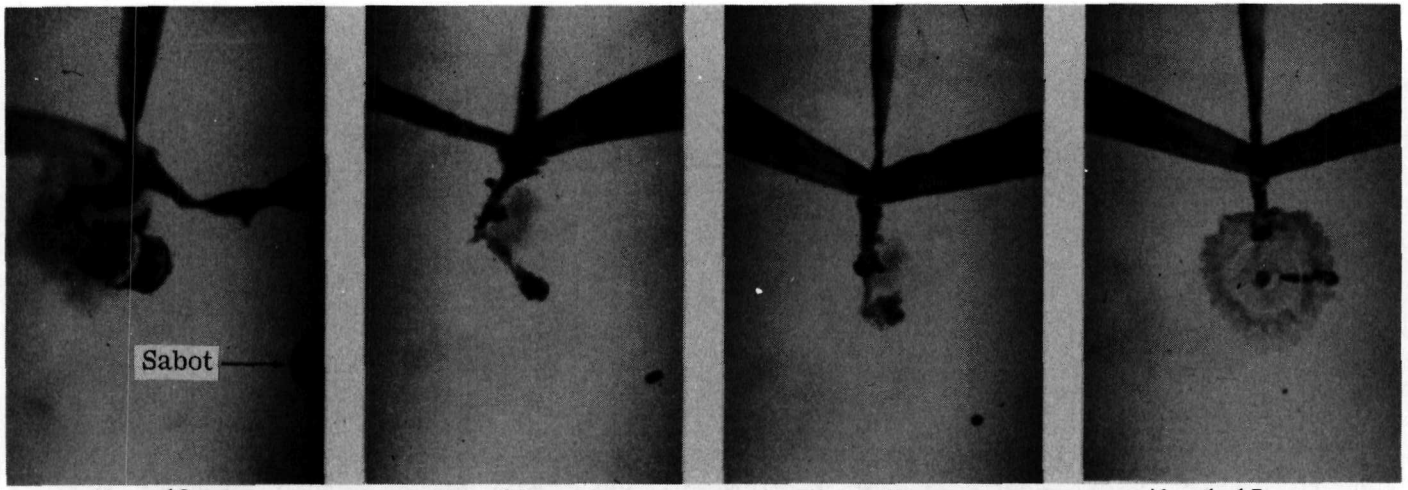

t' = .13 sec t' = .39 sec t' = .55 sec t' = 1.15 sec

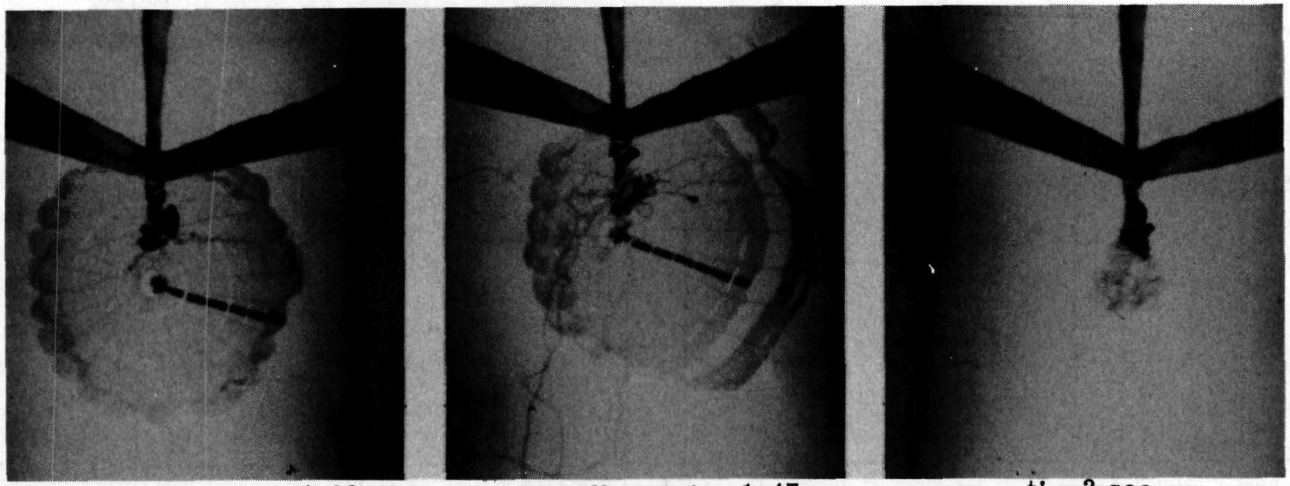

first line failure, t' = 1.32 sec canopy collapse, t' = 1.47 sec t' = 3 sec

L-71-548

Figure 24.- Payload camera photographs of modified ringsail parachute during flight test 6.

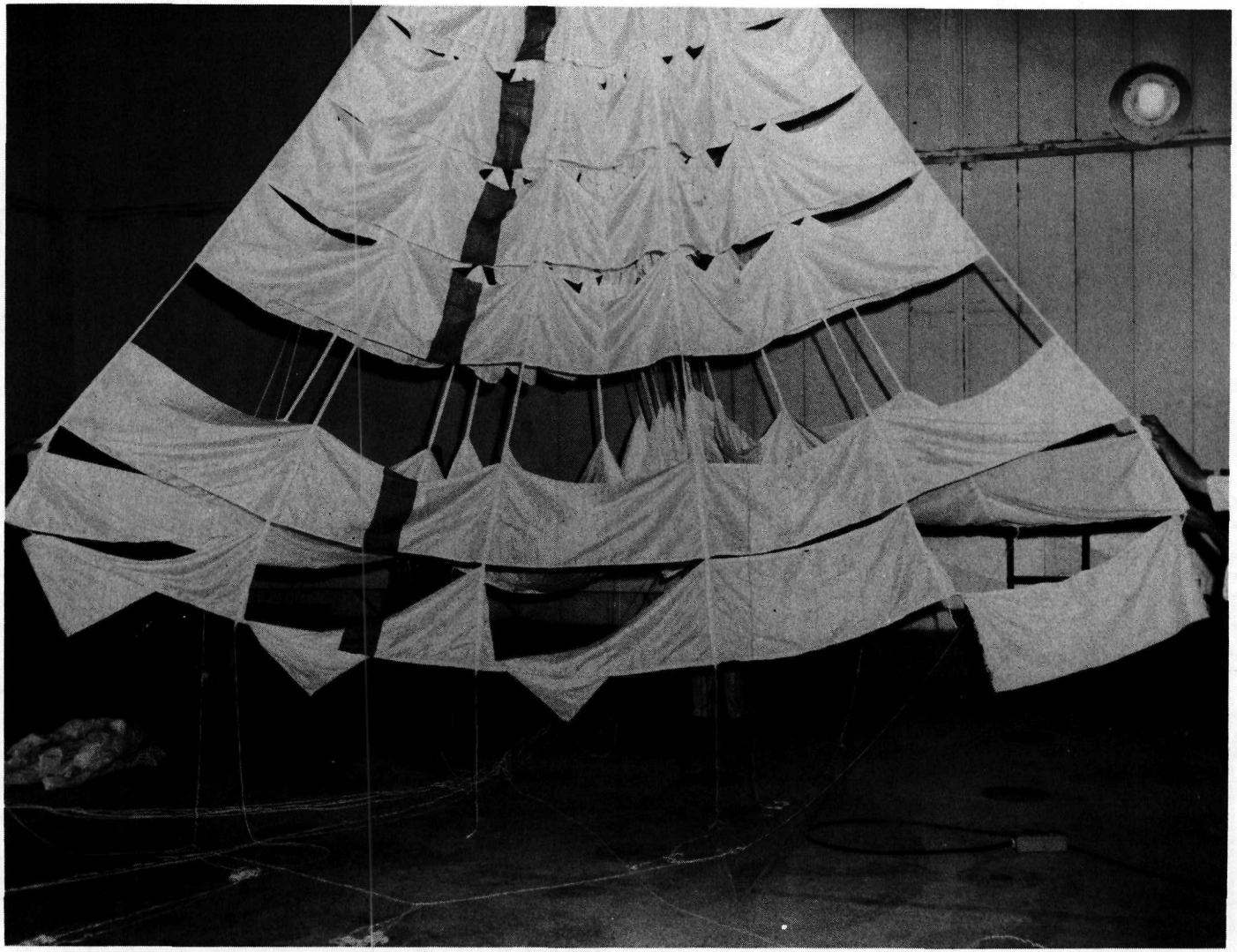

L-71-549

Figure 25.- Canopy damage to 9.5-m-nominal-diameter (31.2 ft) modified ringsail parachute during flight test 6. U.S. Navy photograph.

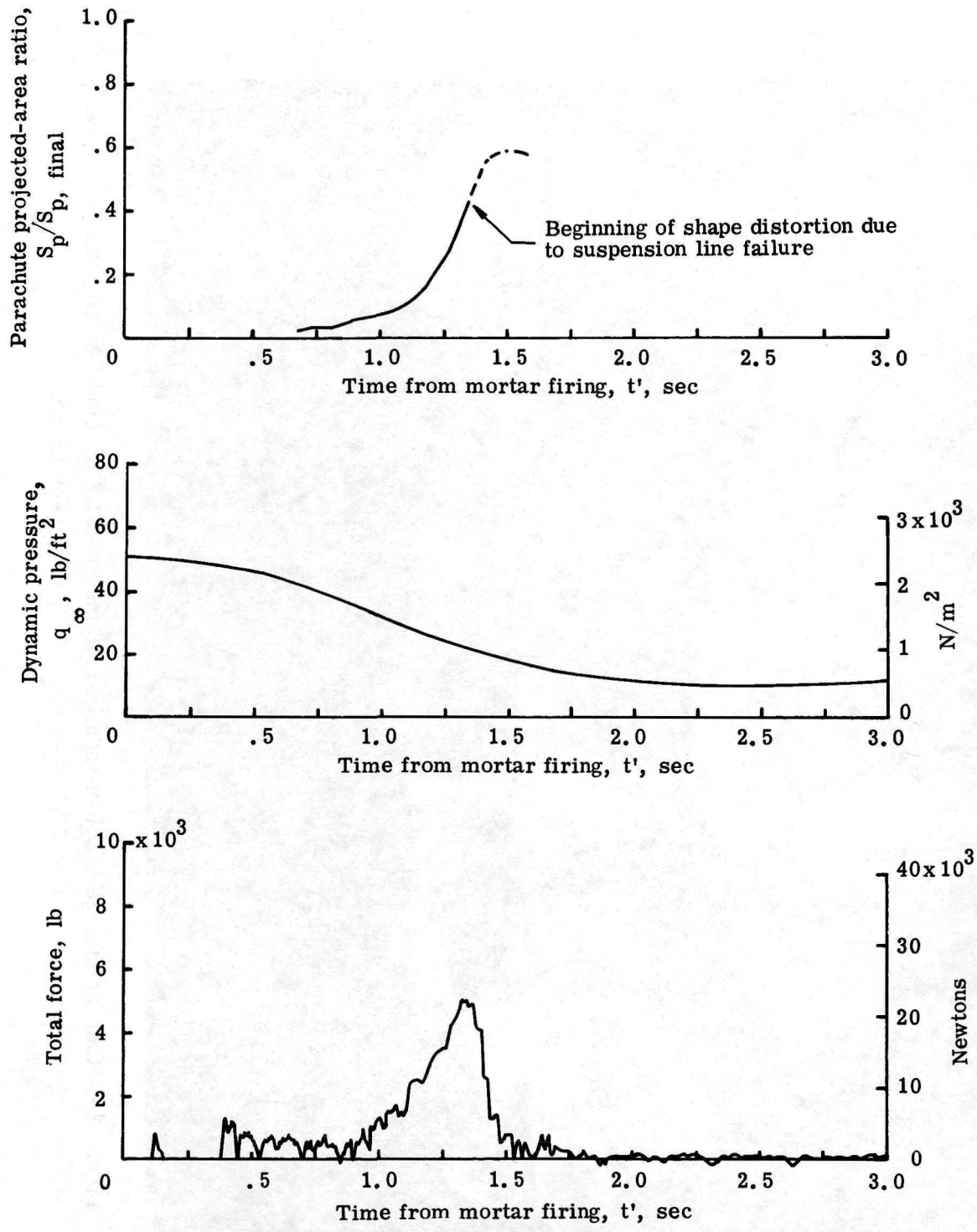

Figure 26.- Time history of the modified ringsail parachute projected-area ratio, dynamic pressure, and total force from flight test 6.

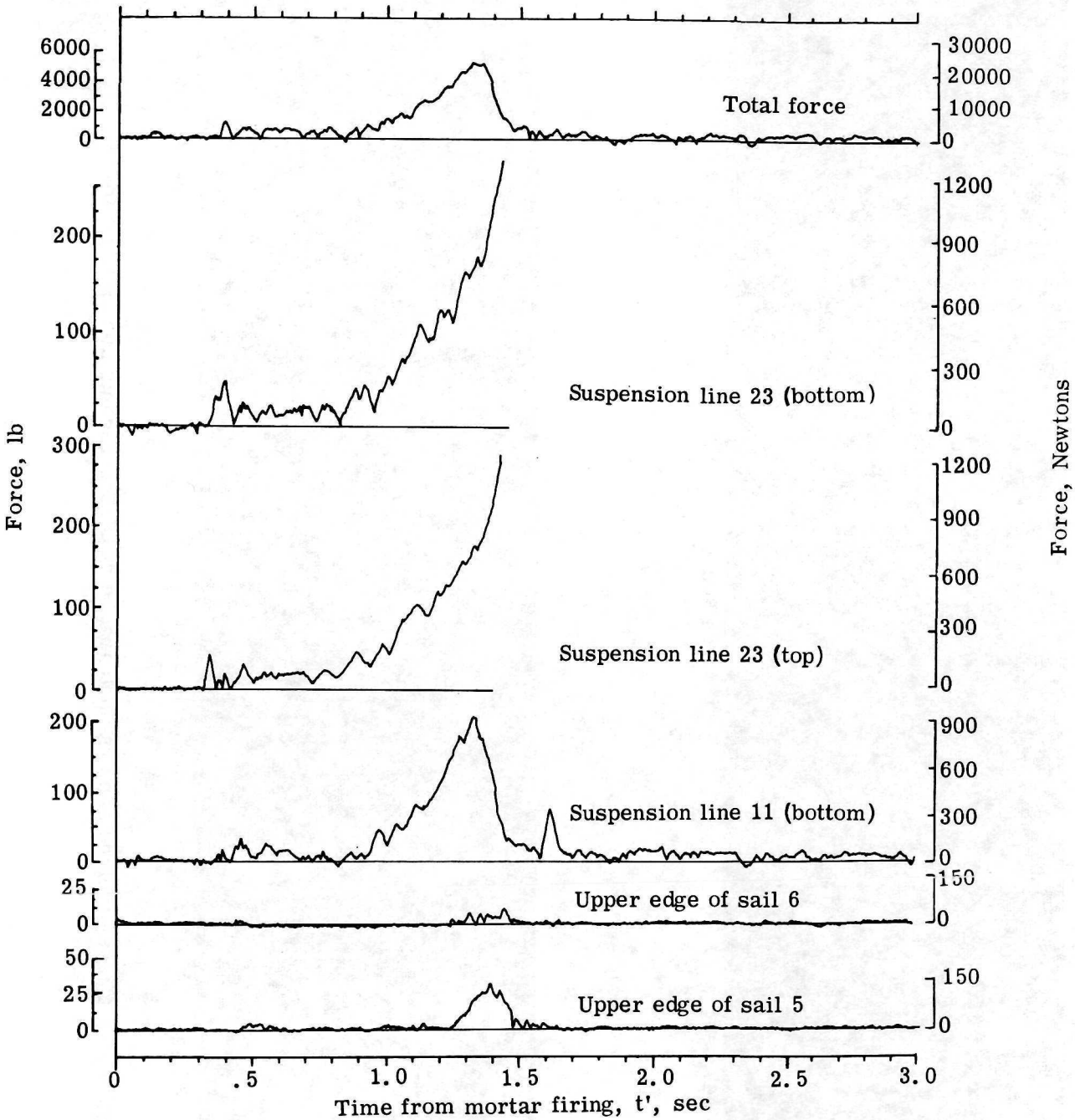

Figure 27.- Force time histories of modified ringsail parachute from flight test 6.

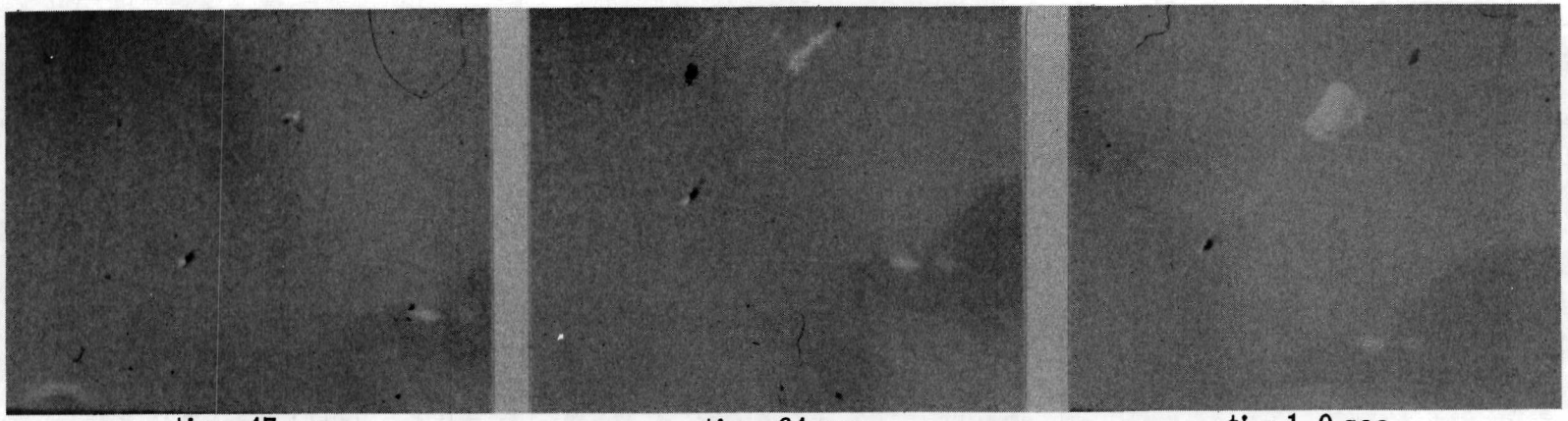

t' = .47 sec t' = .64 sec t' = 1.0 sec

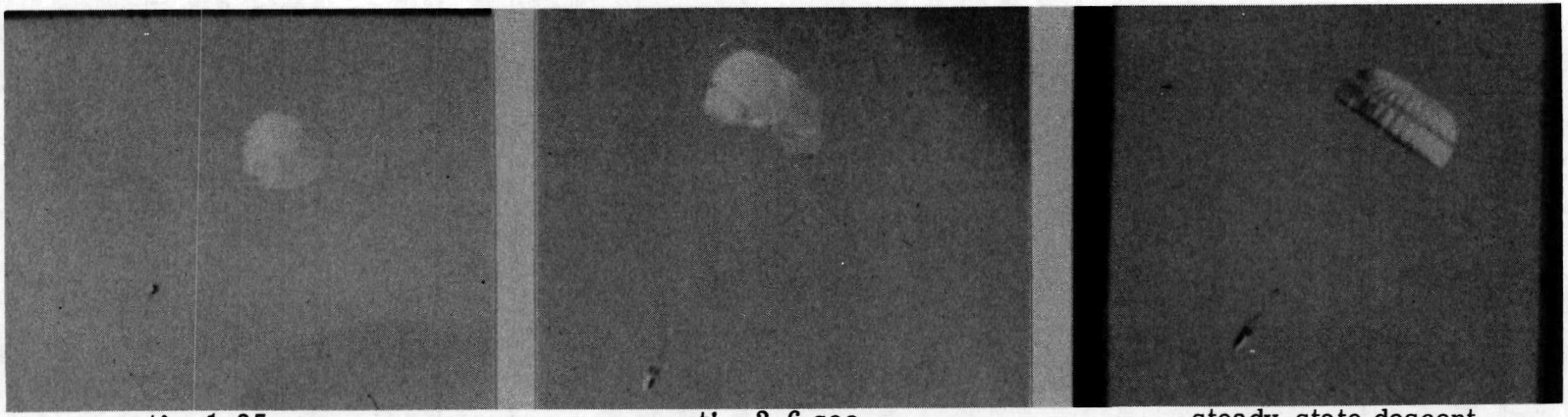

t' = 1.35 sec t' = 2.6 sec steady-state descent

L-71-550

Figure 28.- Chase airplane camera photographs of DGB parachute during flight test 5.

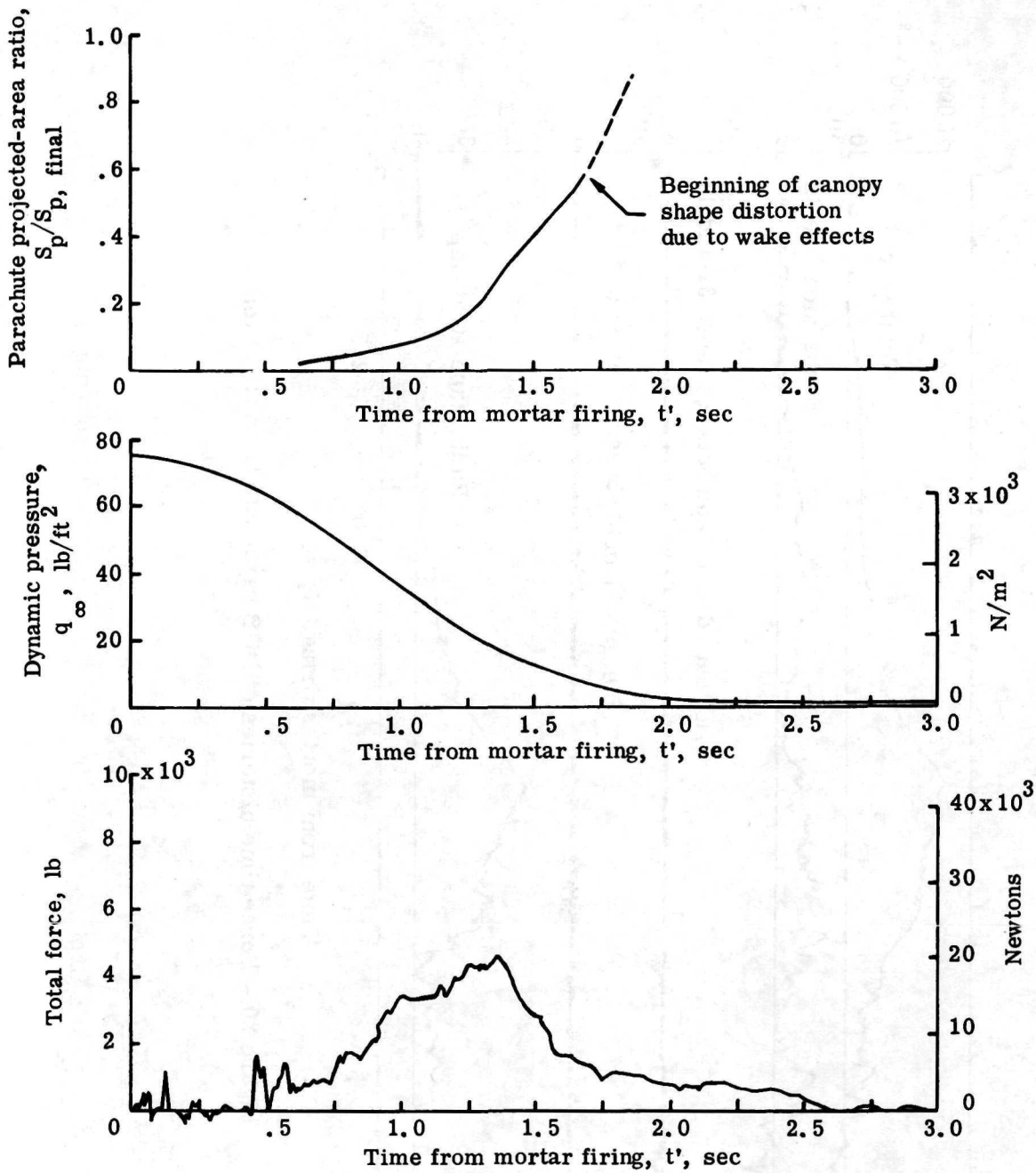

Figure 29.- Time history of the DGB parachute projected-area ratio, dynamic pressure, and total force from flight test 5.

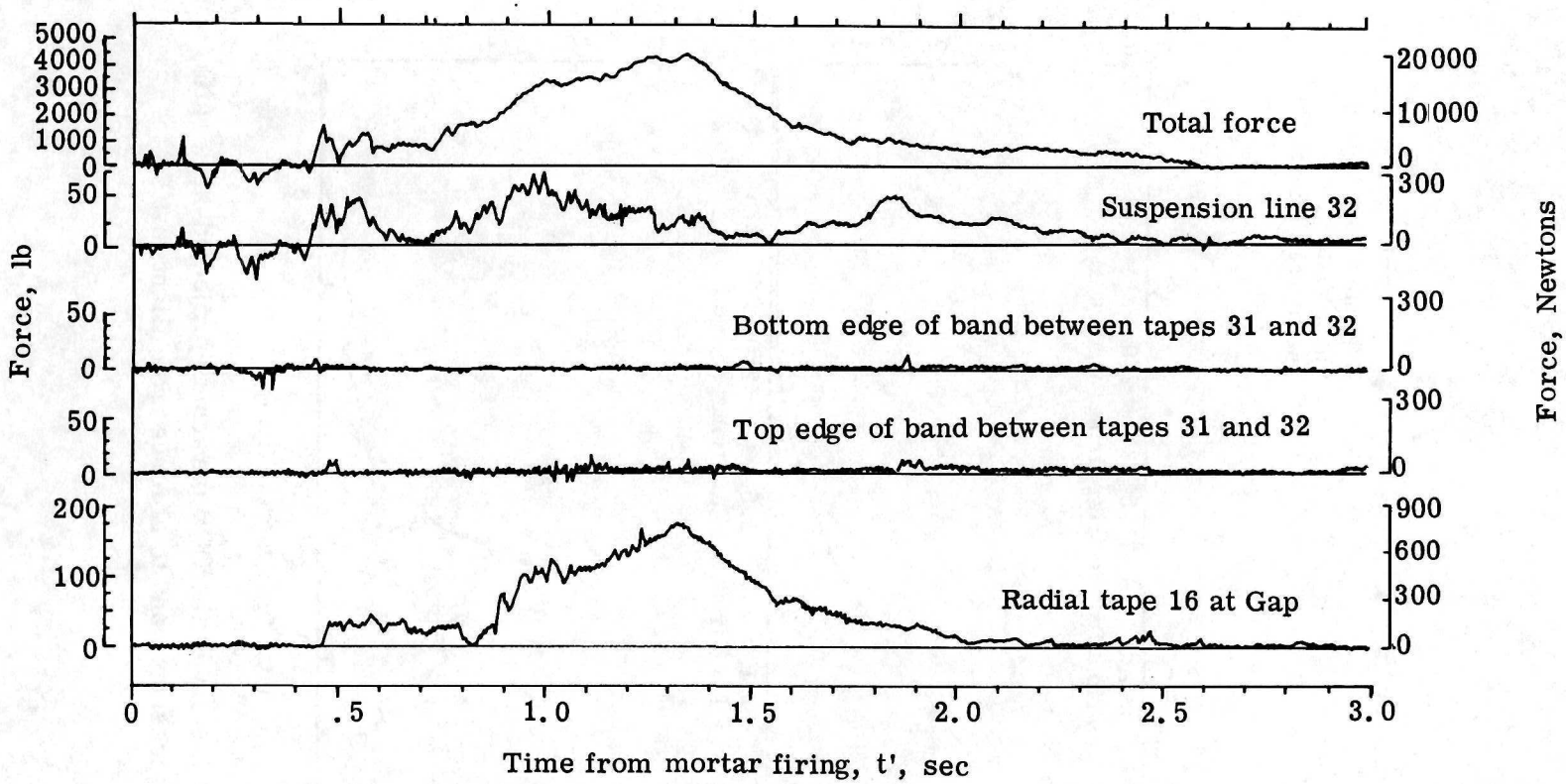

Figure 30.- Force time histories of DGB parachute from flight test 5.

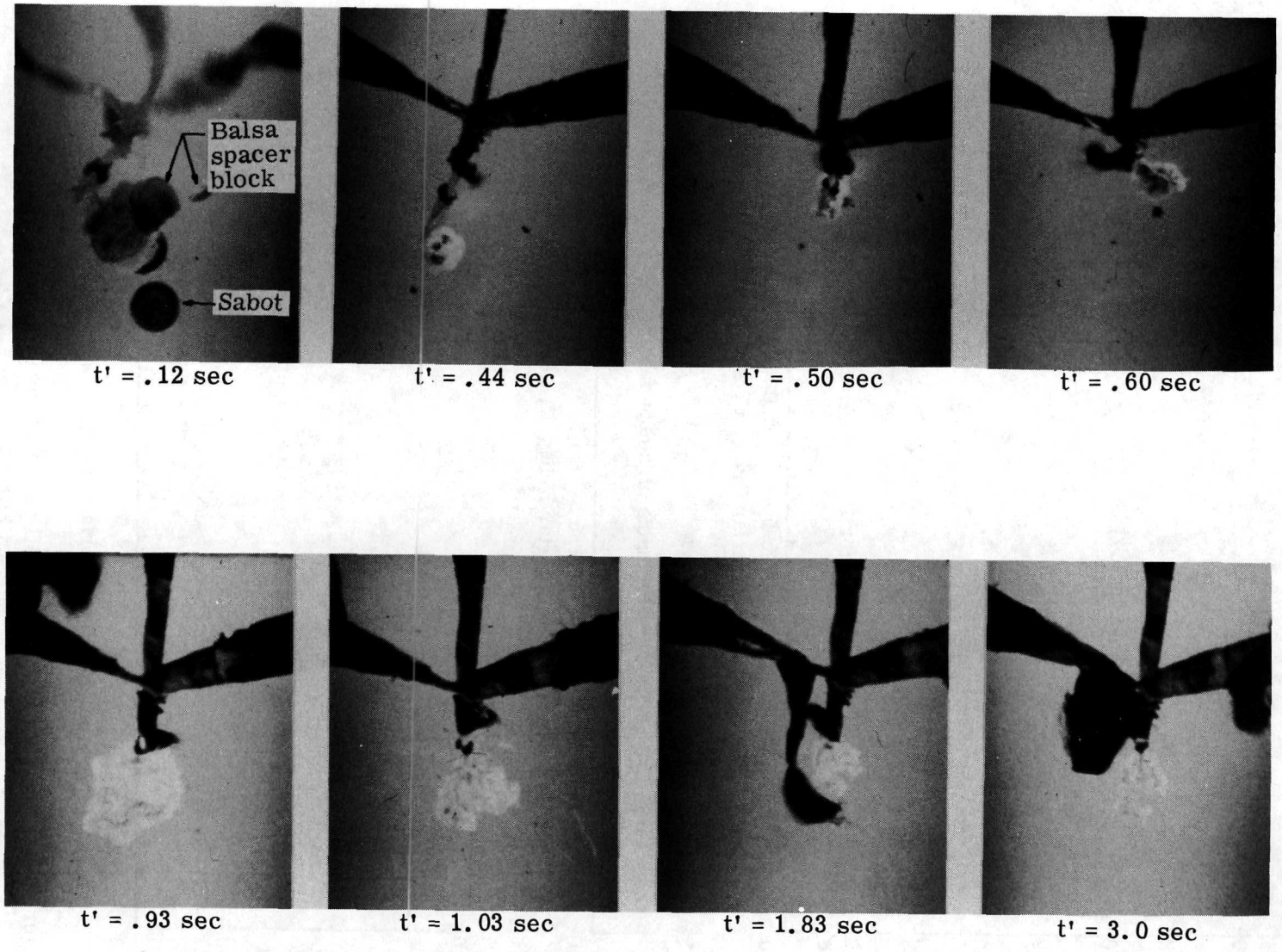

L-71-551

Figure 31.- Payload camera photographs of DGB parachute during flight test 8.

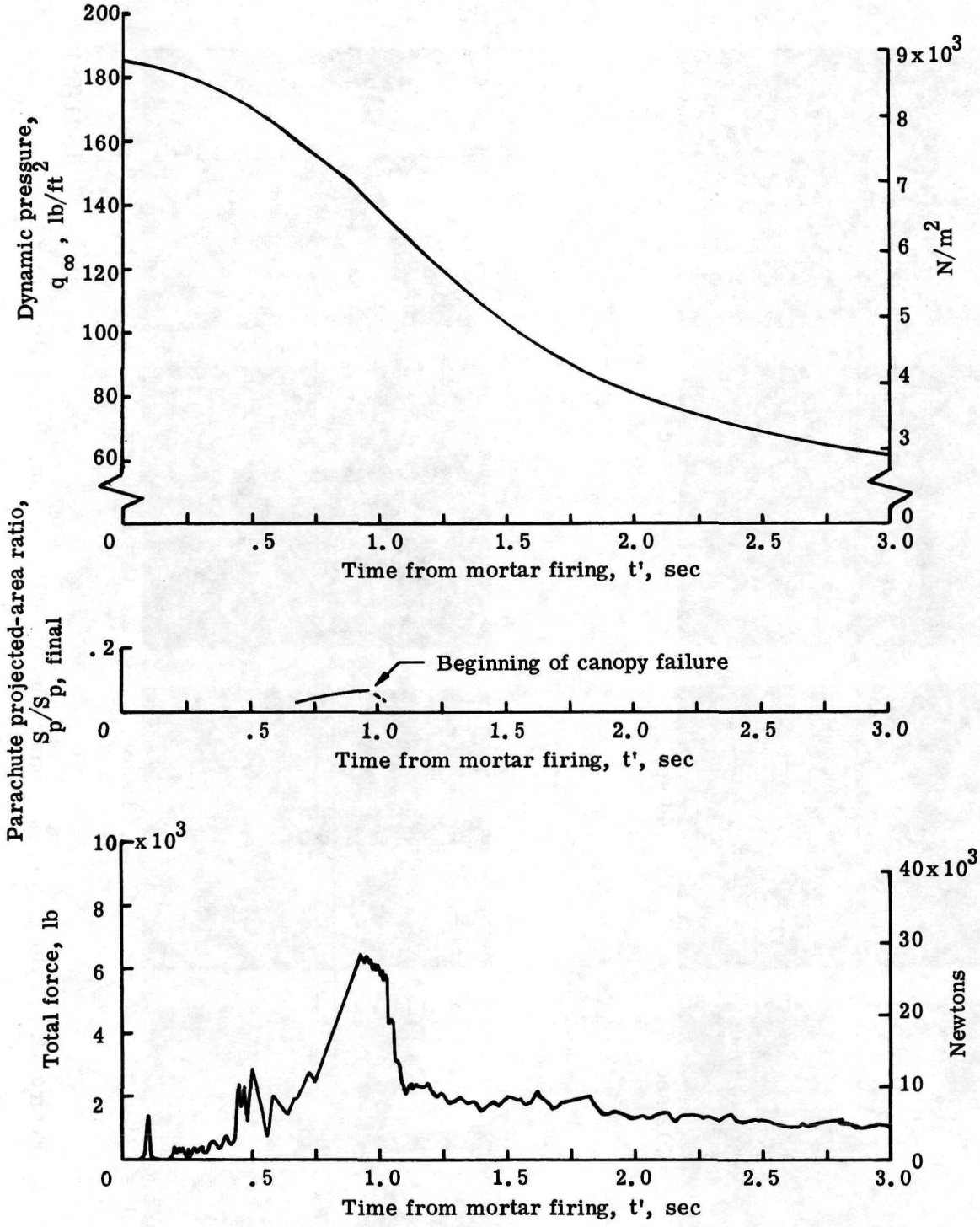

Figure 32.- Time history of the DGB parachute projected-area ratio, dynamic pressure, and total force from flight test 8.

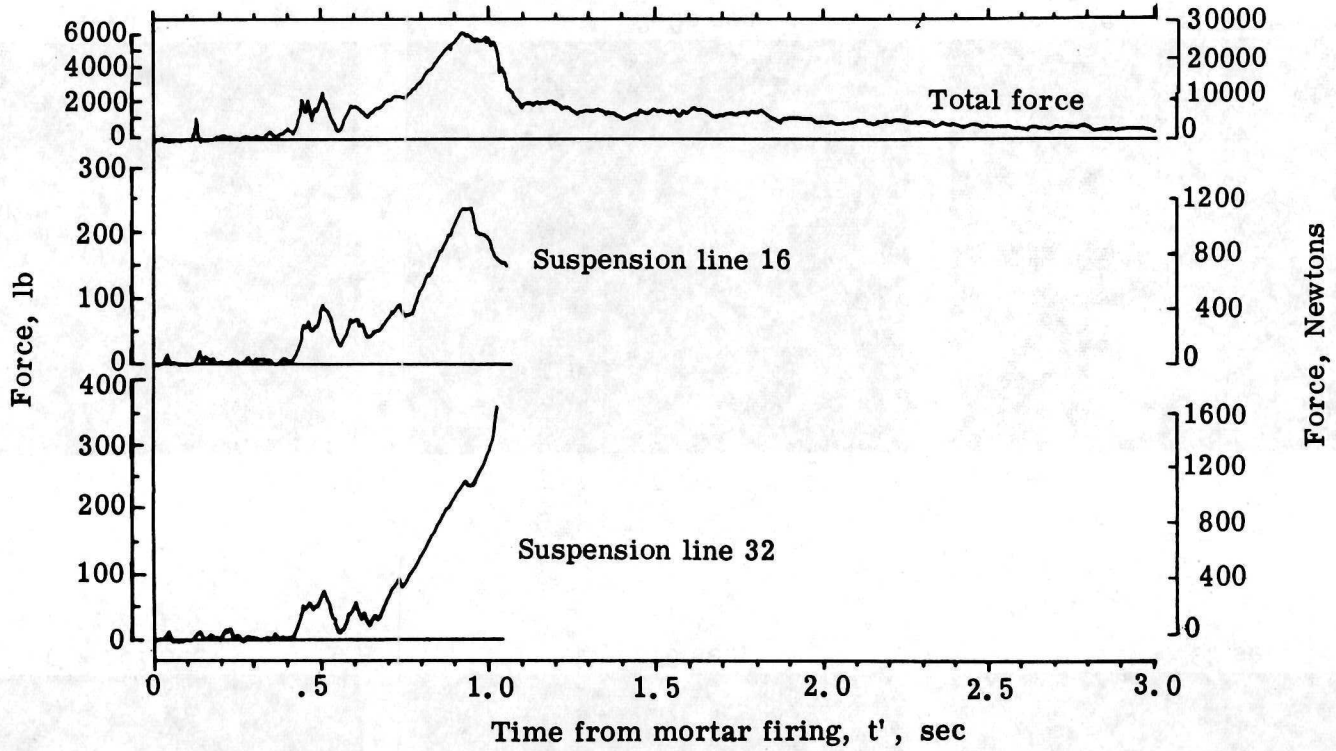

Figure 33.- Force time histories of DGB parachute from flight test 8.

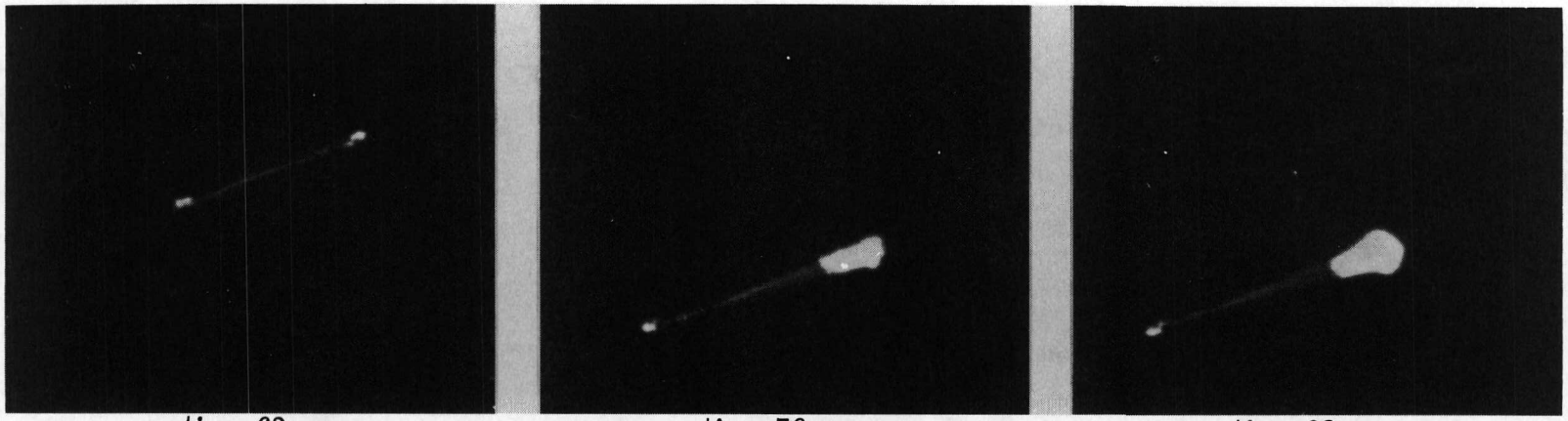

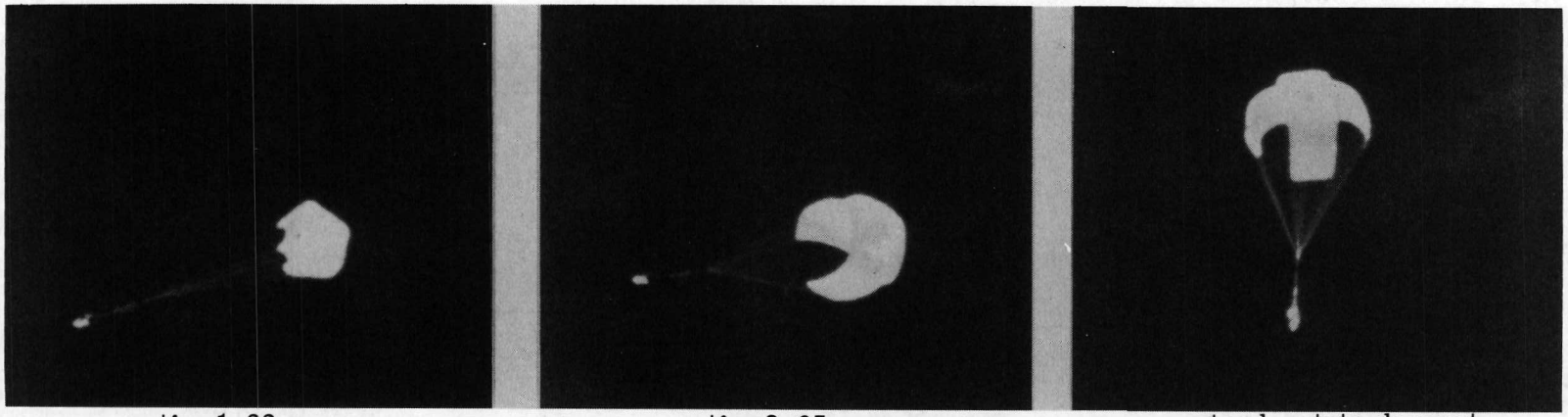

L-71-552

Figure 34.- Ground-based camera photographs of cross parachute during flight test 10.

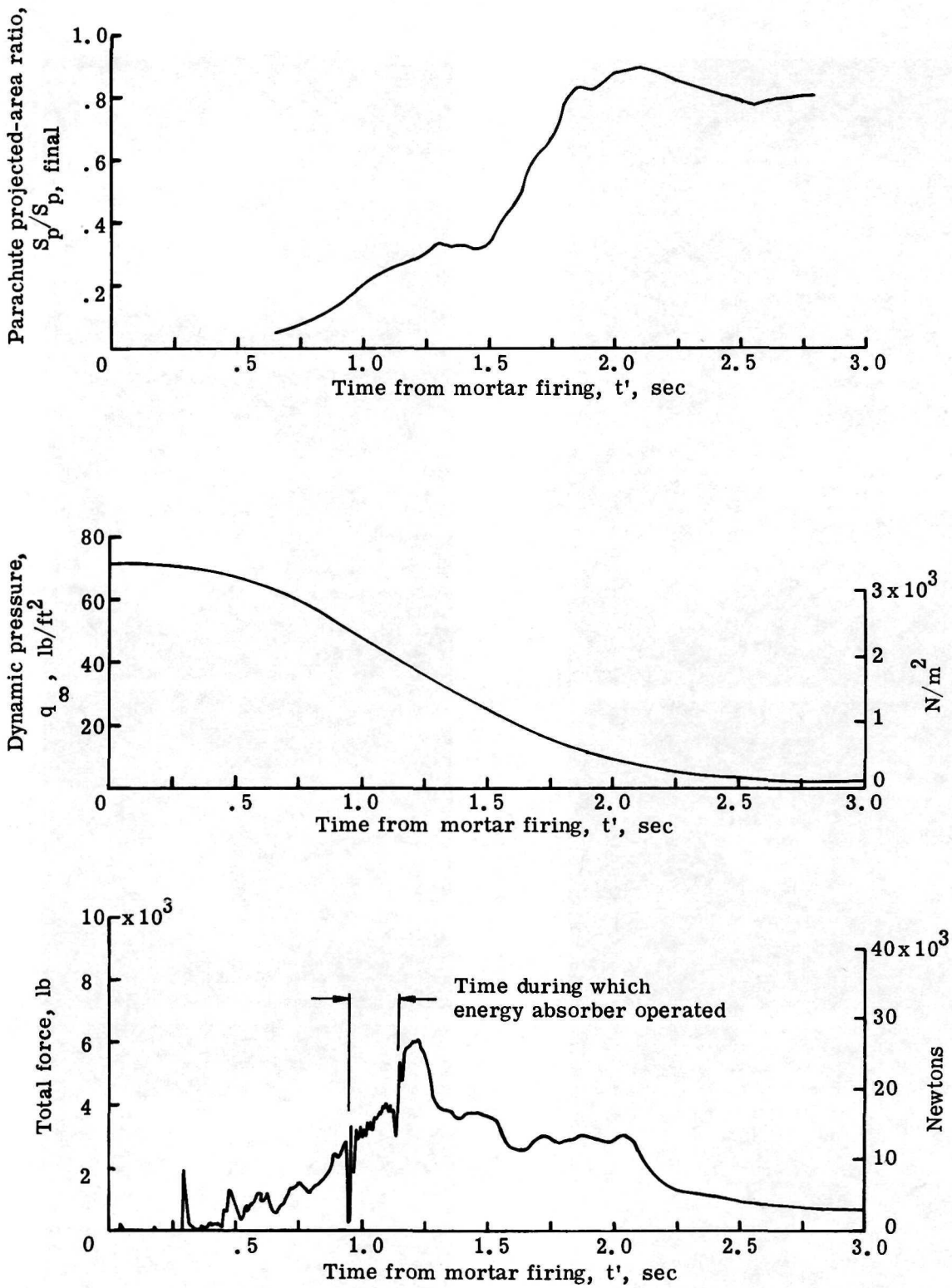

Figure 35.- Time history of the cross parachute projected-area ratio, dynamic pressure, and total force from flight test 10.

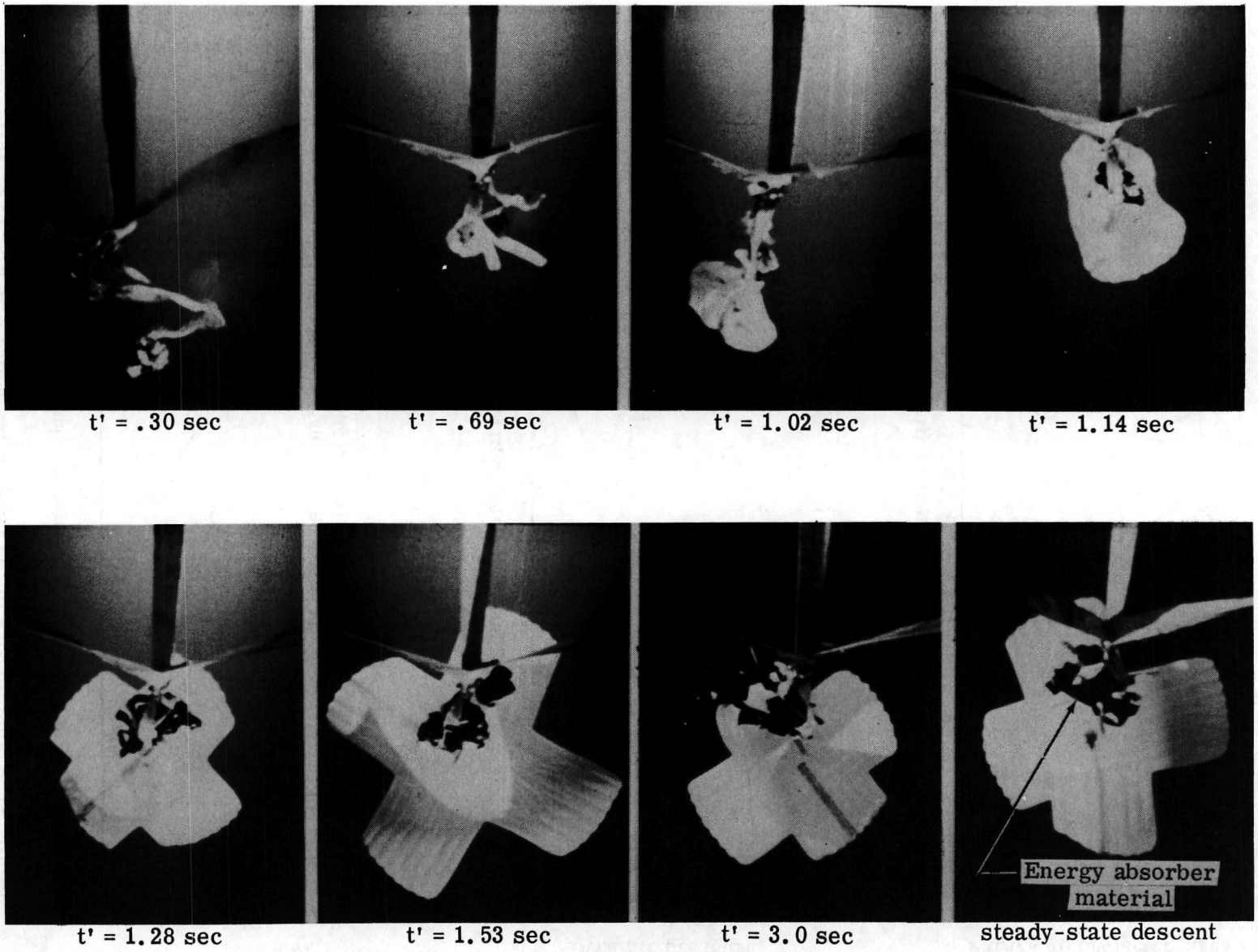

Figure 36.- Payload camera photographs of cross parachute during flight test 11.

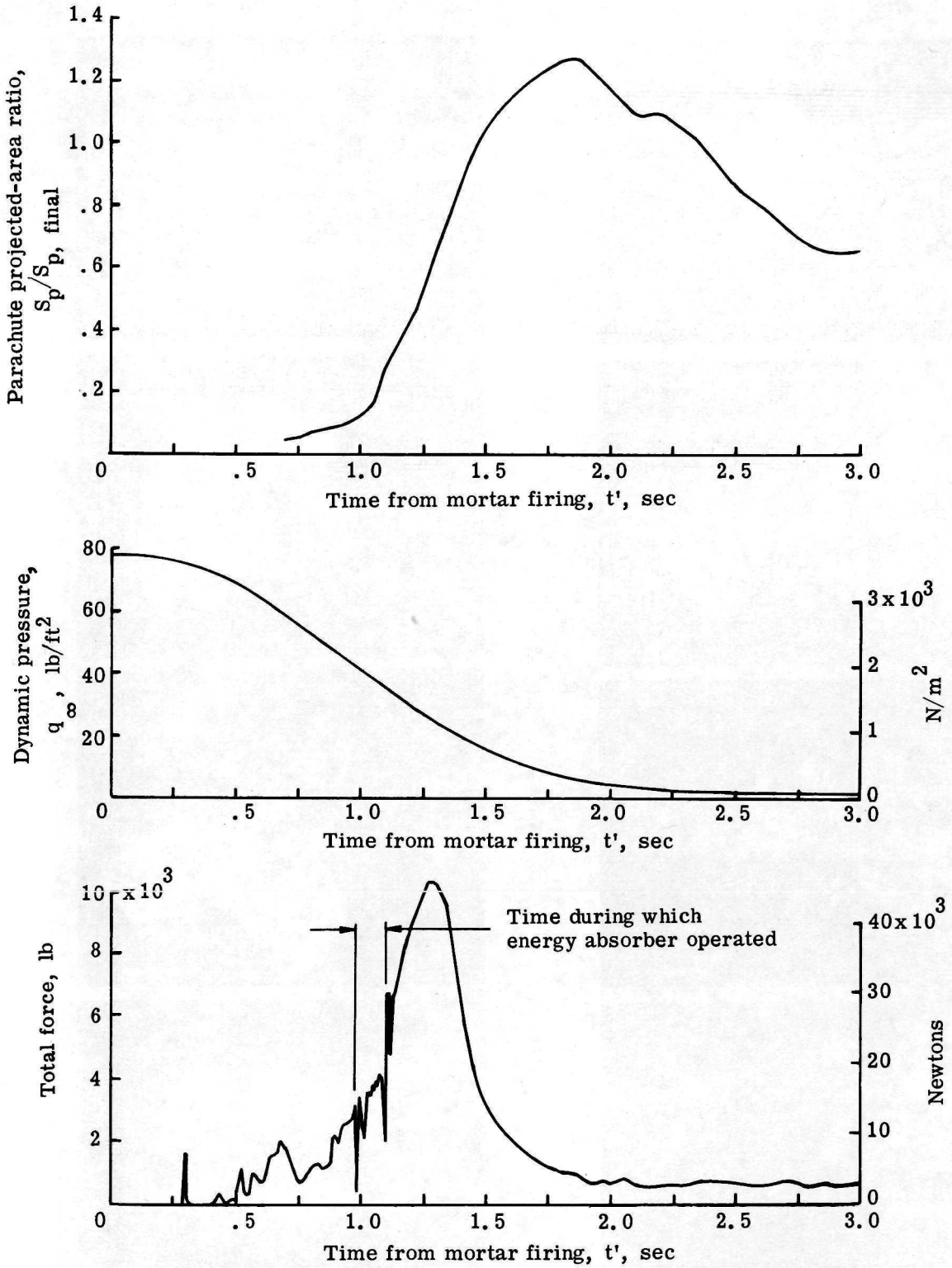

Figure 37.- Time history of the cross parachute projected-area ratio, dynamic pressure, and total force from flight test 11.

"The aeronautical and space activities of the United States shall be conducted so as to contribute . . . to the expansion of human knowledge of phenomena in the atmosphere and space. The Administration shall provide for the widest practicable and appropriate dissemination of information concerning its activities and the results thereof."

— NATIONAL AERONAUTICS AND SPACE ACT OF 1958

NASA SCIENTIFIC AND TECHNICAL PUBLICATIONS

TECHNICAL REPORTS: Scientific and technical information considered important, complete, and a lasting contribution to existing knowledge.

TECHNICAL NOTES: Information less broad in scope but nevertheless of importance as a contribution to existing knowledge.

TECHNICAL MEMORANDUMS: Information receiving limited distribution because of preliminary data, security classification, or other reasons.

CONTRACTOR REPORTS: Scientific and technical information generated under a NASA contract or grant and considered an important contribution to existing knowledge.

TECHNICAL TRANSLATIONS: Information published in a foreign language considered to merit NASA distribution in English.

SPECIAL PUBLICATIONS: Information derived from or of value to NASA activities. Publications include conference proceedings, monographs, data compilations, handbooks, sourcebooks, and special bibliographies.

TECHNOLOGY UTILIZATION PUBLICATIONS: Information on technology used by NASA that may be of particular interest in commercial and other non-aerospace applications. Publications include Tech Briefs, Technology Utilization Reports and Technology Surveys.

Details on the availability of these publications may be obtained from:

SCIENTIFIC AND TECHNICAL INFORMATION OFFICE

NATIONAL AERONAUTICS AND SPACE ADMINISTRATION

Washington, D.C. 20546